2011

A Multiscale Model Of The Neonatal Circulatory System Following Hybrid Norwood Palliation

Andres Ceballos
University of Central Florida

A MULTISCALE MODEL OF THE NEONATAL CIRCULATORY SYSTEM FOLLOWING HYBRID NORWOOD PALLIATION

by

ANDRES CEBALLOS
B.S. University of Central Florida, 2009

A thesis submitted in partial fulfillment of the requirements
for the degree of Master of Science
in the Department of Mechanical, Materials, and Aerospace Engineering
in the College of Engineering and Computer Science
at the University of Central Florida
Orlando, Florida

Summer Term
2011

Major Professor: Alain Kassab

ABSTRACT

Hypoplastic left heart syndrome (HLHS) is a complex cardiac malformation in neonates suffering from congenital heart disease and occurs in nearly 1 per 5000 births. HLHS is uniformly fatal within the first hours or days after birth as the severely malformed anatomies of the left ventricle, mitral and aortic valves, and ascending aorta are not compatible with life. The regularly implemented treatment, the Norwood operation, is a complex open heart procedure that attempts to establish univentricular circulation by removing the atrial septum (communicating the right and left ventricle), reconstructing the malformed aortic arch, and connecting the main pulmonary artery into the reconstructed arch to allow direct perfusion from the right ventricle into the systemic circulation. A relatively new treatment being utilized, the Hybrid Norwood procedure, involves a less invasive strategy to establish univentricular circulation that avoids a cardiopulmonary bypass (heart-lung machine), deliberate cardiac arrest, and circulatory arrest of the patient during the procedure. The resulting systemic-pulmonary circulation is unconventional; blood is pumped simultaneously and in parallel to the systemic and pulmonary arteries after the procedure. Cardiac surgeons are deeply interested in understanding the global and local hemodynamics of this anatomical configuration. To this end, a multiscale model of the entire circulatory system was developed utilizing an electrical lumped parameter model for the peripheral or distal circulation coupled with a 3D Computational Fluid Dynamics (CFD) model to

understand the local hemodynamics. The lumped parameter (LP) model is mainly a closed loop circuit comprised of RLC compartments that model cardiac function as well as the viscous drag, flow inertia, and compliance of the different arterial and venous beds in the body. A system of 32 first-order differential equations is formulated and solved for the LP model using a fourth-order adaptive Runge-Kutta solver. The output pressure and flow waveforms obtained from the LP model are imposed as boundary conditions on the CFD model. Coupling of the two models is done through an iterative process where the parameters in the LP model are adjusted to match the CFD solution. The CFD model domain is a representative HLHS anatomy of an infant after undergoing the Hybrid Norwood procedure and is comprised of the neo-aorta, pulmonary roots, aortic arch with branching arteries, and pulmonary arteries. The flow field is solved over several cardiac cycles using an implicit-unsteady RANS equation solver with the k-epsilon turbulence model.

To friends, family and everyone who's made my life richer. Special dedication to Martha, Marcelo, Daniel and my late father Nestor, to whom I owe every bit of engineer in me.

ACKNOWLEDGMENTS

Special thanks to:

My mentors Dr. Eduardo Divo, Dr. Alain Kassab and Dr. William DeCampli for their support, motivation and inspiration. Ruben Osorio and Dr. Ricardo Agueta-Morales for their important contributions to this work and to the Cardiovascular Engineering Research Team at UCF.

TABLE OF CONTENTS

LIST OF FIGURES

LIST OF TABLES

CHAPTER 1
INTRODUCTION

Congenital heart disease is the leading cause of death for infants born with birth defects, with more than a 30% mortality attributed to this disease. One of the most complex forms of congenital heart disease is HLSH and occurs in 4 to 8 percent of infants born with cardiac malformations [7]. The main complications of HLHS are severely malformed anatomies of the left ventricle, mitral and aortic valves, and ascending aorta 1.1. There are currently two approaches to therapy for children with HLSH: heart transplantation or surgical intervention to establish univentricular circulation. Unfortunately heart transplantation is often not an alternative due to the low number of donors at this early age [8]. Surgical techniques such as the Norwood operation are then the most common method to establish an early blood circulation that is compatible with life. The Norwood operation consists of removal of the atrial septum, reconstruction the malformed aorta, and connection of a bypass (BT-shunt) from the innominate artery to the right pulmonary artery (RPA) to allow for pulmonary perfusion 1.1.

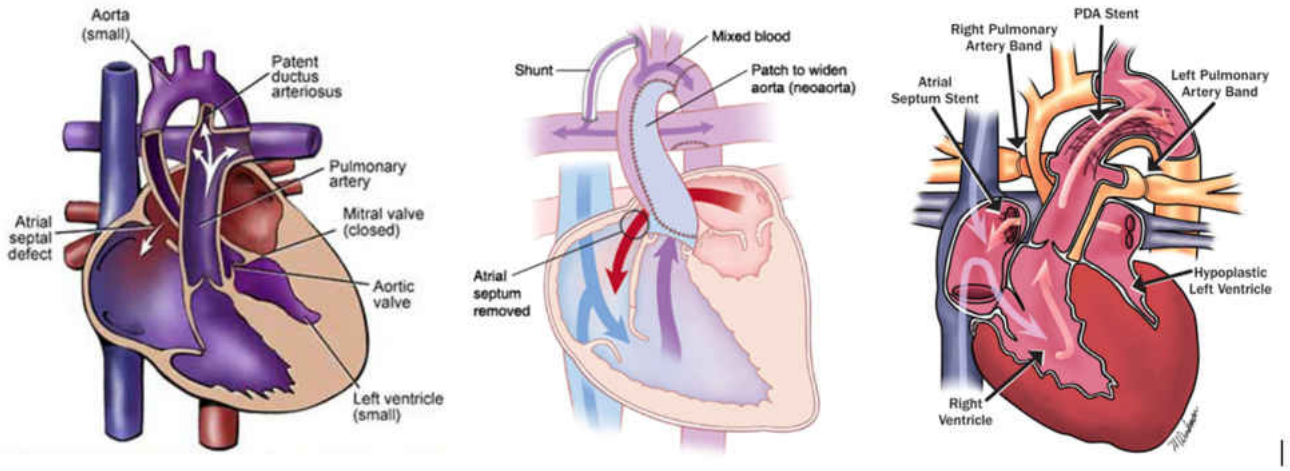

Figure 1.1: HLHS Anatomy (left)[1], Standard Norwood Anatomy (center)[2], Hybrid Norwood Anatomy (right)[3]

Successful recovery of the patient from the Norwood operation is often followed by subsequent surgical procedures to establish a more normal circulatory system where pulmonary perfusion is achieved with deoxygenated blood. A relatively new alternative to the first-stage Norwood procedure is the Hybrid Norwood procedure, which consists of removal of the atrial septum, implantation of a stent in the patent ductus arteriosis, and banding of the pulmonary arteries . The PDA, a small vessel that connects the pulmonary arteries with the aortic arch and normally closes shortly after birth, is enlarged with the use of the stent to allow circulation from the right ventricle into the systemic circulation through the aortic arch. The pulmonary banding is put in place to prevent excessive pulmonary circulation, with an ideal adjustment providing a pulmonary to systemic flow ratio of 1 [9]. The Hybrid Norwood is a less invasive procedure that avoids the use of a heart-lung machine as well as deliberate cardiac and circulatory arrest. Though there are numerous surgical advantages of the Hybrid versus the conventional method, there are also different complications that may

arise with this method. The most important to surgeons participating in this study is the obstruction of flow due to stenosis of the aortic arch proximal to the stent. This condition is fatal if coronary and/or carotid flow is critically low. With the expectation of increasing perfusion to these vessels, a bypass called Reverse BT-shunt (RBTS) is placed connecting the pulmonary root to the innominate artery 1.2.

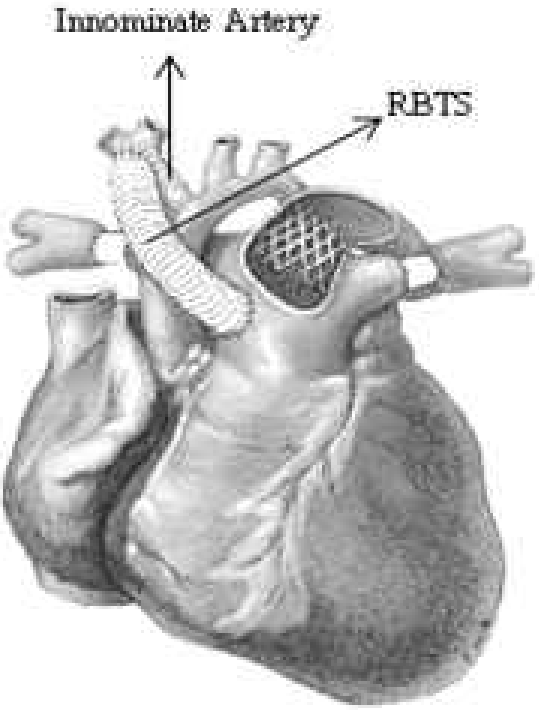

Figure 1.2: Hybrid Norwood Anatomy with RBTS in place

The resulting hemodynamics are very complex since the flow reaching the innominate artery is both antegrade and retrograde, meaning part of the circulation flows downstream through the innominate and part upstream to feed the coronary and remaining aortic branches. Furthermore, flow reversal and secondary motions have been detected throughout the cardiac cycle, making this circulatory configuration far from intuitive [10]. Surgeons are

therefore deeply interested in understanding the local hemodynamics of the with RBTS in place Hybrid Norwood anatomy and the potential benefits of the reverse BT shunt, especially when severe stenosis is present. The main objectives of this study are therefore: 1) To develop a closed-loop, multiscale model of the cardiovascular system able to describe detailed local hemodynamics and its effects on the global circulation; 2) assess the performance of the RBTS in increasing perfusion to the coronary and carotid circulation.

CHAPTER 2

RELEVANT ANATOMICAL AND PHYSIOLOGICAL FEATURES OF THE CARDIOVASCULAR SYSTEM

In humans, the cardiovascular system is composed of the heart and a closed system of vessels constituted by the arteries, veins and capillaries. The primary function of the cardiovascular system is the transport of oxygen, carbon dioxide, nutrients, hormones and other life essential nutrients[6]. There are two primary blood circuits, the pulmonary and the systemic circuits. The pulmonary circuit is composed of the pulmonary arteries and its branches that deliver blood from the right ventricle to the lungs, the capillaries in the lungs where gas exchange occurs, and the pulmonary veins that deliver oxygen rich blood to the left atrium. The systemic circuit supplies nutrients to all tissues in the body and its vessels include the aorta and branching arteries which distribute the blood coming from the left ventricle, the capillary system through which material exchange occurs, and the systemic veins that return the blood to the heart[5].

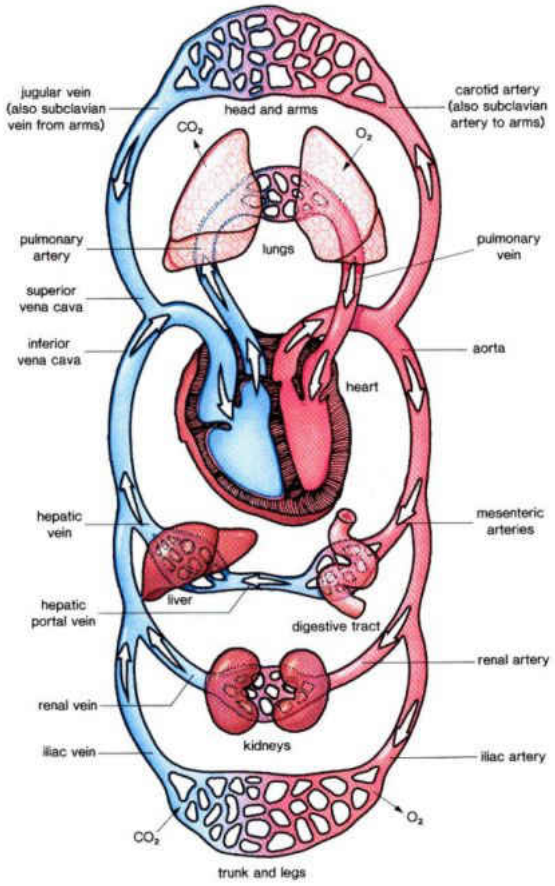

Figure 2.1: The Circulatory System (The Internet Encyclopedia of Science [4])

2.1 THE HEART

Basic Heart Anatomy The heart is a muscular pump that sustains the flow of blood through the body. It does so in a periodic cycle of events denominated the cardiac cycle. It has four chambers, two atria and two ventricles; the left supports the systemic circulation and the right the pulmonary circulation. The left and right side of the heart are separated by the atrial and ventricular septums. In a healthy heart, the systemic and pulmonary circulations occur in parallel, with deoxygenated blood flowing through the right heart and oxygenated

blood through the left heart. The heart's walls are mainly composed of three layers of tissue and muscle. The outermost layer is the epicardium, a serous membrane which is not easily distensible and thus restricts excessive and rapid expansion of the cardiac chambers. Lining the interior chambers of the heart is the endocardium, a smooth layer of tissue extending over the heart valves. In between the epicardium and endocardium is the myocardium, the muscle that enables the heart's contraction and is made of muscular fibers of variable thicknesses within the different chambers. The left ventricle is much more developed than the right ventricle, with a thicker wall allowing for higher ventricular pressures required to provide adequate systemic perfusion. Four valves allow filling of the chambers and prevent regurgitation. The right atrium is supplied by the inferior and superior venae cava and blood flows through the mitral valve into the right ventricle. Blood is then pumped through the pulmonary valve into the main pulmonary artery. Similarly, the left atrium is supplied by the pulmonary veins and blood flows through the tricuspid valve into the left ventricle. Blood is then pumped through the aortic valve into the ascending aorta. The myocardium is perfused by the coronary arteries, relatively narrow vessels that feed from the root of the ascending aorta, immediately above the aortic valve. There are two principal coronary arteries, the left and right coronary arteries, that branch around their respective ventricles[5].

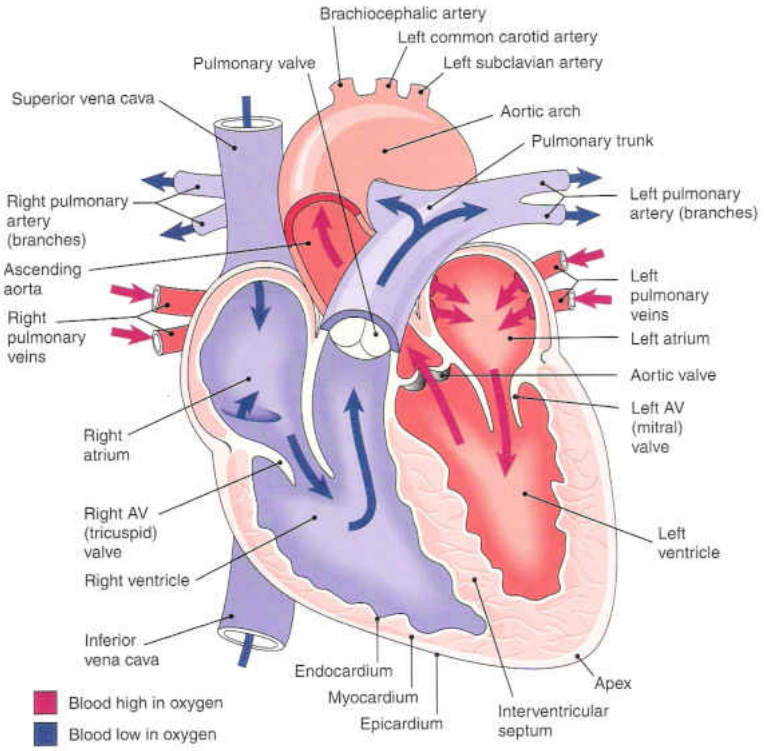

Figure 2.2: Healthy Heart Anatomy [5]

2.2 THE CARDIAC CYCLE

The cardiac cycle can be briefly defined as the sequential contraction and relaxation of the atria and ventricles[6]. The periods of contraction and relaxation are denominated systole and diastole, respectively. Below is a description of the cardiac cycle stages.

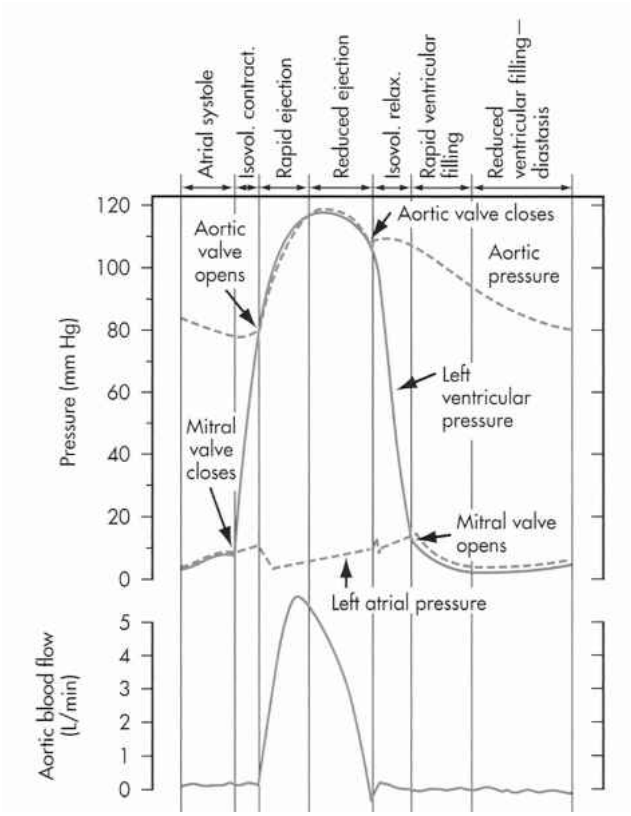

Figure 2.3: Cardiac Output of the Systemic Circulation [6]

Ventricular Systole

- Isovolumic Contraction: this is the period after the ventricle has just been filled and the atrioventricular and semi-lunar valves are closed. There is marked intraventricular pressure increase at constant volume.
- Ejection: begins when the intraventricular pressure exceeds the arterial pressure and the semi-lunar valve opens. Immediately after the valve opening there is rapid ejection and a continued rise in ventricular and aortic pressure. Due to the arterial wall compliance, some of the pulse energy is stored in the arterial walls and then released after peak systolic pressure. Flow inertia drives a subsequent period of reduced ejection

from the ventricle, in which the ventricular-aortic pressure gradient starts reversing and the arterial walls begin contracting. Eventually the arterial pressure exceeds that of the ventricle and the semi-lunar valve closes. A small amount of flow reverses through the aortic valve as it closes, producing a small region of negative cardiac output as seen in Figure 2.3.

Ventricular Diastole

- Isovolumic Relaxation: the closure of the aortic valve after the period of reduced ejection produces the incisura, also called the anacrotic notch, on the onset of diastole. The pressure within the ventricle is still higher than that in the atrium, therefore both valves are closed and the sharp reduction of pressure is isovolumic.
- Rapid Filling: at the end stages of ventricular relaxation the pressure in the ventricle becomes less than that in the atrium causing the atrioventricular valves to open. The blood that had filled the ventricle during ventricular diastole now rushes into the ventricle rapidly and there is a marked increase in ventricle pressure and volume.
- Diastasis: as the ventricle fills its pressure increases gradually until it reaches the atrial pressure at which point the atrioventricular valve begins to close.

Atrial Systole This is the period of atrial contraction, which elevates the atrial pressure beyond that of the ventricle allowing the atrioventricular valve to open and the filling of the ventricle. Usually this produces an additional 20% of ventricular filling after diastole during rest and even a higher percentage during exercise due to higher flow inertia.

2.3 VESSEL ANATOMY AND PHYSIOLOGY

2.3.1 ARTERIES

There are three types of vessels that transport oxygenated blood through the body: the arteries, arterioles, and capillaries. All arteries have a basic composition of an internal or intimal layer that is directly in contact with the circulation, a middle layer containing smooth muscle cells, and an outer layer composed of elastin, colagen fibers, and other connective tissue (Figure 2.4). The intimal layer, or tunica intima, is mainly composed of the endothelium, a thin layer of cells that facilitate the flow of blood and are responsible for the release of anticoagulation and vasoregulatory substances. The middle layer, or tunica media, is responsible for the contraction or dilation of the vessel under stimuli. It also has a layer of elastic tissue that supports and allows the vessel to contract after a pressure pulse. The outer layer or tunica adventitia maintains the vessel in place.

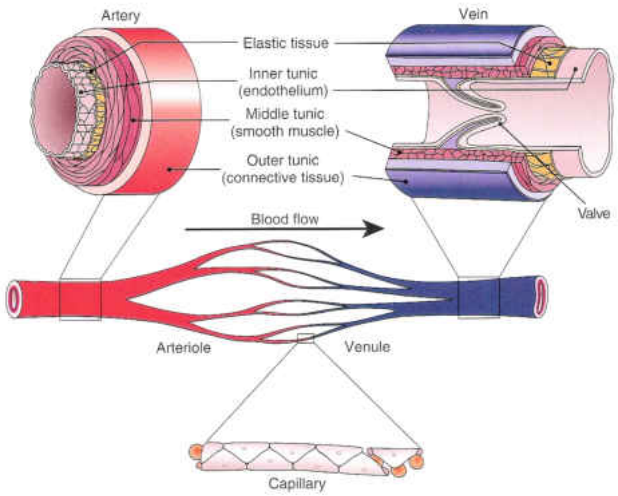

Figure 2.4: Arterial and Venous Composition [5]

The arteries can be subdivided in two major groups:

- Elastic arteries: these are the largest arteries in the body and are typically 1 to 2.5 cm in diameter. Arteries within this group include the pulmonary artery, aorta and its major branching arteries. The higher proportion of elastine in the tunica media in these vessels gives them higher compliance than in vessels of smaller diameter and therefore can "store" flow during systole.
- Muscular arteries: these are vessels in the range of 1mm to 1cm in diameter. The tunica media in these vessels contains a higher proportion of smooth muscle, which allows them to constrict or distend to regulate blood flow.

The arterioles are smaller in diameter (0.01 - 1 mm) than muscular arteries and contain less elastic and connective tissue. These vessels control to great extent the regulation of blood pressure and do so with a relatively higher amount of smooth muscle that varies the crossectional area of the lumen. The smallest vessels in the body (0.005 mm, - 0.01mm) are the capillaries through which material exchange occurs. Their walls are very thin, about 1 cell thin to enable diffusion. Flow velocity through the capillaries is very slow relative to arterial flow due to the increased equivalent crossectional area of their lumen.

2.3.2 VEINS

The vessels that return blood flow from the arterial system to the heart can be divided into two groups, the veins and venules. Venules are the smallest vessels in the venous system (0.005mm - 0.1mm) and their walls are continuous with those of the capillaries. They share some of the physiological properties and are very similar wherever material exchange occurs.

The venules transport the blood to larger vessels, the veins, which increase in diameter, wall thickness, and composition as they approach the heart (0.1mm - 20mm). Typically veins have thinner walls when compared to arteries of the same lumen since they are subjected to much lower pressures and wave amplitudes. At the point where blood reaches the veins, much of the mechanical energy that drives the flow has been spent. To aid the return of blood to the heart, most veins have valves that prevent retrograde flow. Contraction of muscles in the extremities and the changes in pressure in the torso due to breathing also help to drive the flow to the heart.

2.3.3 FLOW CHARACTERISTICS THROUGH THE ARTERIAL AND VENOUS SYSTEM

As described earlier, the composition of the arterial and venous walls varies depending on their size and location. As the composition of the vessels change so do their mechanical properties. Elasticity is perhaps the most important property of the blood vessels in the present study. In the arterial system, the relatively high elasticity in the larger arteries allows them to store some kinetic energy of the flow during systole, as evidenced by their distension, and release it during diastole. This property, which will be referred to as compliance, will be explained further in Section 4.3. This achieves three things: a more continuous flow to the tissues, a reduction in pressure wave amplitude, and a reduction in cardiac workload. The further downstream through the arterial system, the more attenuated is the pressure waveform and the more steady flow becomes. Once the blood reaches the capillary beds it encounters high resistance to flow, as the equivalent vessel crossectional area increases and

the flow slows down to allow diffusion to occur. The result is near steady flow through the capillary beds. This effect is denominated the "hydraulic filter" in reference to the effects of capacitance and resistance in electrical circuits, which analogous to this case dampen the pressure and flow waveform signals from the heart.

CHAPTER 3
HLHS AND THE HYBRID NORWOOD ANATOMY

3.1 HLHS ANATOMY

Hypoplastic Left Heart Syndrome (HLHS) comprises a group of malformations and underdevelopment of the left side of the heart. These include an underdeveloped left atrium and ventricle, stenosis or atretia of the aortic and mitral valves, and hypoplasia (in this case significant narrowing) of the ascending aorta [11]. As a consequence there is no ejection from the left ventricle to the ascending aorta. The right heart becomes enlarged and hypertrophic, since it has to support both pulmonary and systemic circulations at the same time. In newborns, the patent ductus arteriosus (PDA) connects the pulmonary artery to the mid-aortic arch, allowing the aforementioned univentricular circulation to be possible. The PDA, however, naturally starts to recede and eventually ceases to exist as a blood conduit shortly after birth. Atrial septal defect (ASD), a malformation that allows blood flow between the two atria, is also present. The systemic and pulmonary circulation are in serial with the HLHS anatomy, since all the blood is pumped by the right ventricle into the main pulmonary artery. Blood flows retrograde through the ascending aorta into the subclavian and coronary arteries.

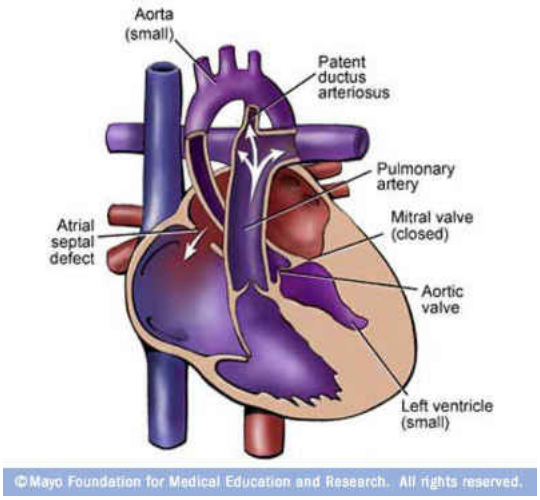

Figure 3.1: HLHS Anatomy [1]

3.2 HYBRID NORWOOD PROCEDURE AND POSTOPERATIVE ANATOMY

3.2.1 THE HYBRID NORWOOD PROCEDURE

The hybrid Norwood procedure was named after Dr. William Norwood, the pioneer of surgical treatment for patients with HLHS. The following is a brief description of the principal objectives of the operation.

Pulmonary Artery Banding The procedure starts with a median sternotomy and placement of a chest retractor. The pericardium is opened and a suture stay is placed to allow the manipulation of the main pulmonary artery (MPA). Two segments of 3.5 mm polytetrafluoroethylene (PTFE) tube grafts (same material used in bypasses) are cut to be used as bands for the left (LPA) and right (RPA) pulmonary arteries[11]. The bands are

placed around the root of the pulmonary arteries and are sutured. If being implemented, a reverse BT-shunt is anastomosed to the innominate artery from the MPA. An angiogram (flow visualization in arteries using X-ray) is performed to confirm placement and proper amount of occlusion, usually about 50% of original lumen.

Ductal Stenting A puncture is made at the root of the MPA where a sheath, the conduit through which the catheter passes, is introduced. A stent, an expandable metallic mesh, is deployed along the entire length of the ductus arteriosus using the catheter. Proper placement of the stent is confirmed using an angiogram after the sheath/catheter is removed. If there is not enough flow crossing the atrial septum a septostomy is performed or a stent is placed to enlarge it. The sternum is closed and a subcuticular suture finishes the operation.

3.2.2 POSTOPERATIVE ANATOMY

Figure 3.2 shows the changes to the anatomy performed after the hybrid Norwood procedure. Univentricular circulation is established through the placement of the PDA stent, the banding of the pulmonary arteries, and if required septostomy or atrial stenting. In this configuration, the systemic and pulmonary circulations are in parallel as both circuits are fed from the MPA. Since the left ventricle is hypoplastic and the aortic valve is essentially shut, inter-communication of the atria must exist in order to allow incoming blood from the pulmonary arteries to reach the right ventricle. This is why there must be an ASD of the proper size or septostomy or stenting must be employed to guarantee this intercommunication. Very important to note is the mixing of oxygenated blood returning from the pulmonary veins

with deoxygenated blood returning from the vena cavae in the atria. This results in both pulmonary and systemic circuits feeding from blood with the same oxygen content. Balancing the pulmonary to systemic blood flow ratios (Qp/Qs) is very important to the recovery of the patient. Studies [12, 13]have shown that the optimal Qp/Qs ratio is 1 for adequate systemic perfusion and metabolic function.

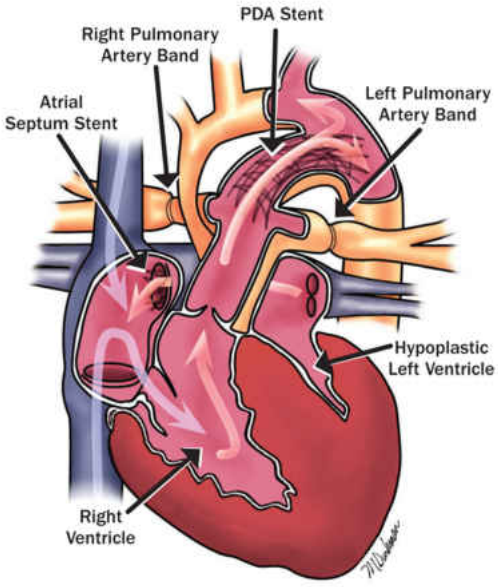

Figure 3.2: Hybrid Norwood Anatomy [3]

3.2.3 POSTOPERATIVE COMPLICATIONS

The Hybrid Norwood procedure has its unique set of complications that may arise during postoperative care:

- Preductal Stenosis - since no ascending aorta reconstruction is performed, stenosis prior to the PDA may restrict retrograde flow and produce insufficient cerebral and coronary perfusion. In addition, it is necessary to place the stent protruding from the

PDA into the isthmus (proximal region in the aortic arch prior to the PDA) to prevent ductal constriction[9]. This may increase the risk of preductal stenosis since the stent itself promotes neointimal proliferation[14]. The degree of stenosis may vary prior to stage two palliation and is one of the variables that is analyzed in the present study.

- Atrial Stent Patency- as reported by Bacha et. al [9], ductal stents are unreliable beyond three months after placement.
- Stent and Pulmonary Band Migration - ductal stent migration can occur into the MPA or descending aorta if an incorrect diameter is chosen or the stent is misplaced. Pulmonary band migration can also occur due to size and placement issues.

CHAPTER 4
MATERIALS AND METHODS

4.1 ANATOMICAL MODEL

The aortic arch anatomy representative of an infant after undergoing the Hybrid Norwood procedure was constructed using SolidWorks (Dassault Systemes, Concord, MA) and includes the pulmonary root (PR), descending aorta (DA), innominate artery (IA), right and left subclavian arteries (RSA, LSA), right and left carotid arteries (RCA, LCA), and right and left coronary arteries (RcorA, LcorA). Three other models were constructed, one with severe stenosis, one with the RBTS, and one with severe stenosis and RBTS (Figure 4.1).

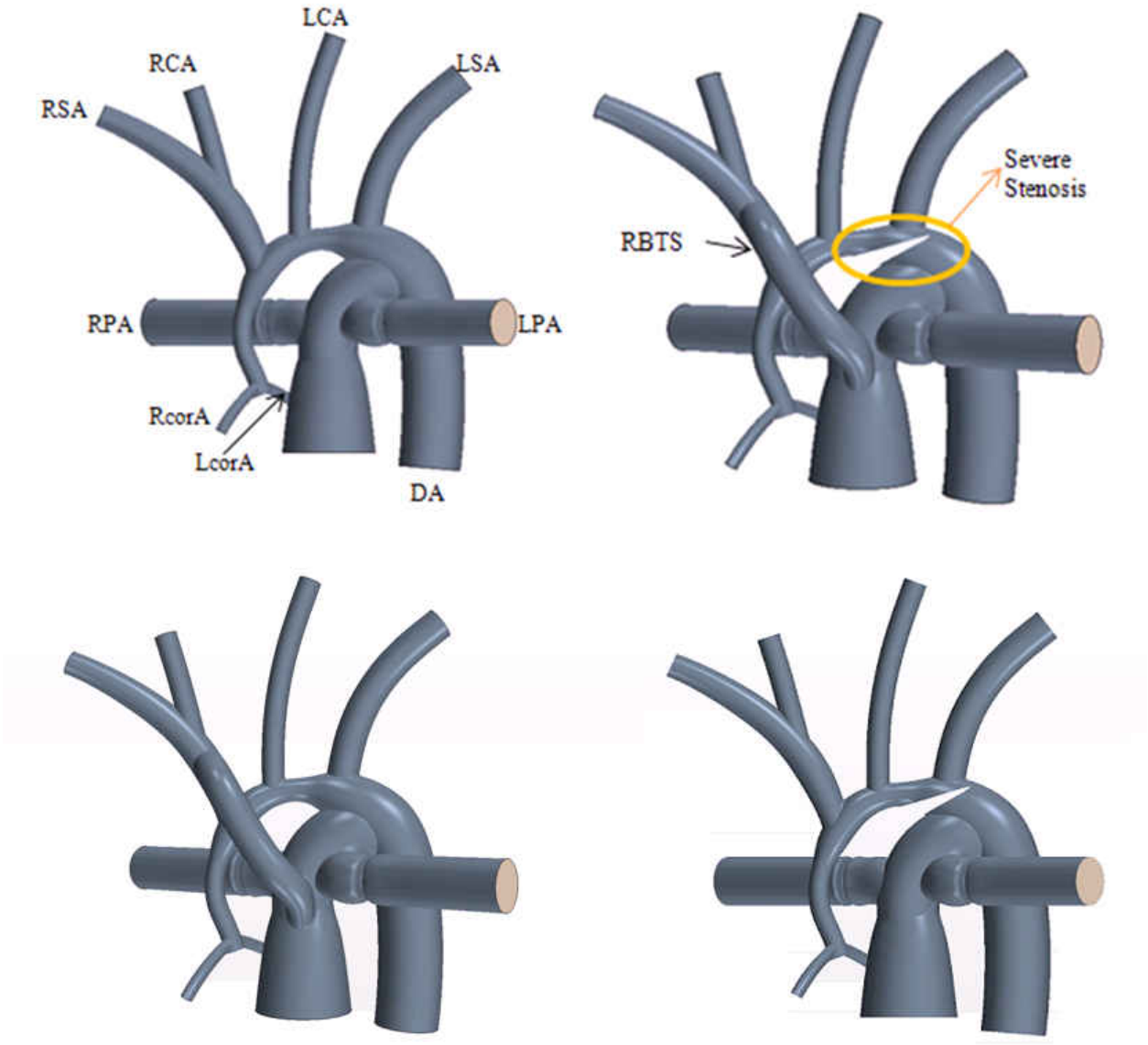

Figure 4.1: Nominal Hybrid Norwood Anatomy (top left); Nominal Hybrid Norwood Anatomy with RBTS (bottom left); Severe Stenosis Anatomy with RBTS in place (right); Severe Stenosis Anatomy (bottom right)

Placement of the RBTS was performed from the PA root just below the RPA and LPA branching into the innominate artery prior to the RSA-LCA branching with a near normal incidence angle (Figure 4.2).

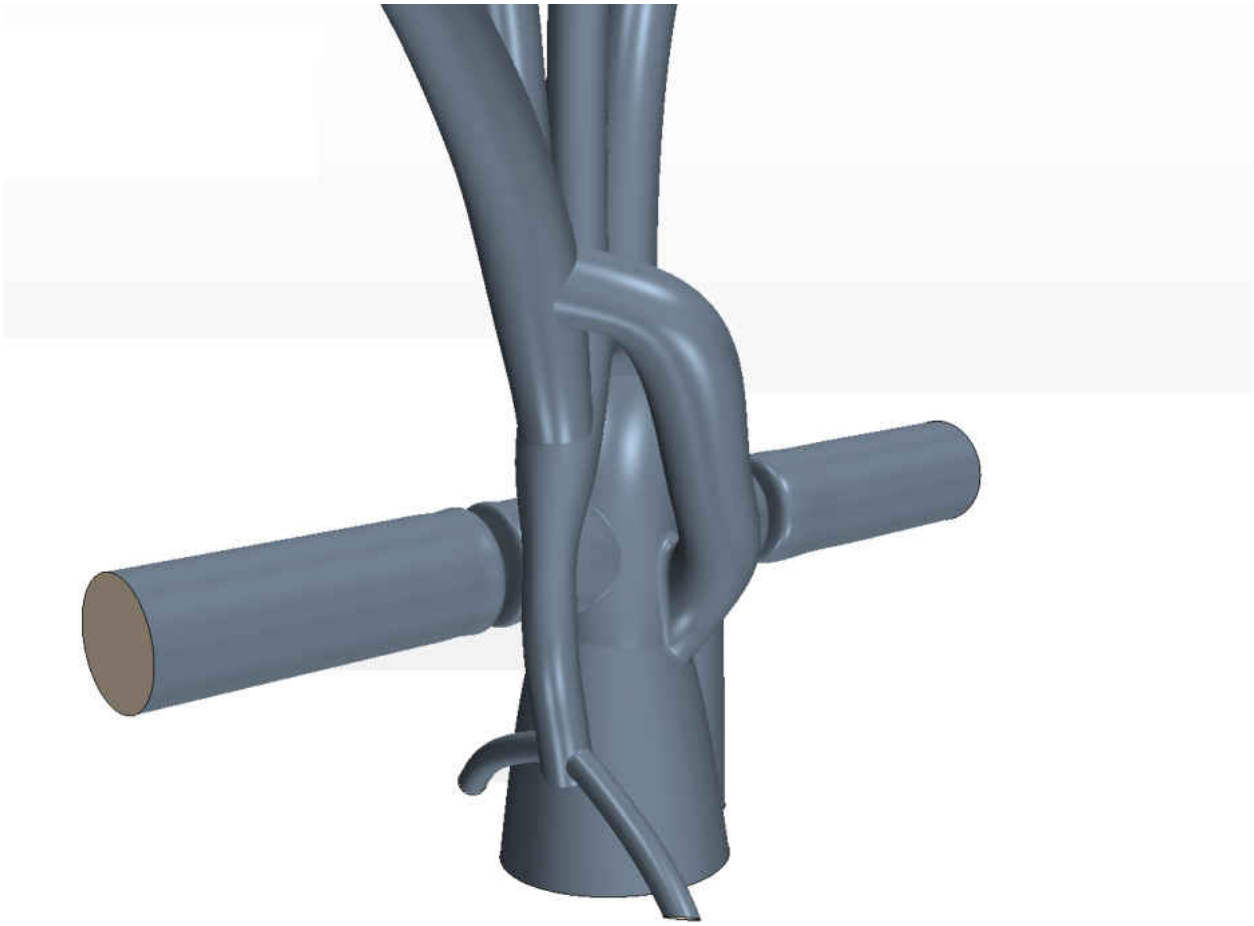

Figure 4.2: RBTS Placement

The severe stenosis was modeled by removing part of the computational domain prior to the ductus arteriosus. The shape was chosen to approximate that of the real occlusion. A reduction in lumen cross-sectional area of 88.3% was produced, from 19.63 mm^2preductal arch lumen to 2.30 mm^2 isthmus lumen.

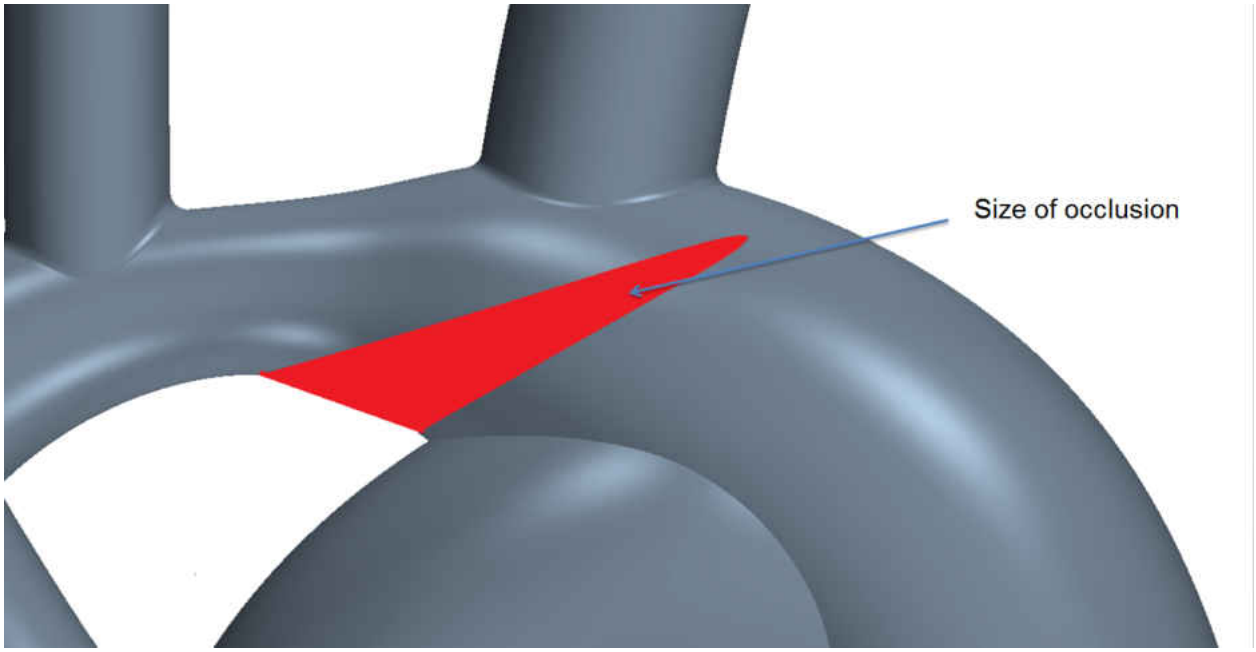

Figure 4.3: Severe Preductal Stenosis

Dimensions and features among the models don't change except for the addition of the RBTS and/or stenosis. Figure 4.4 depicts vessel diameters and important dimensions along the arch, including stenosis. Figure 4.5 depicts the anatomy with RBTS and unoccluded arch dimensions.

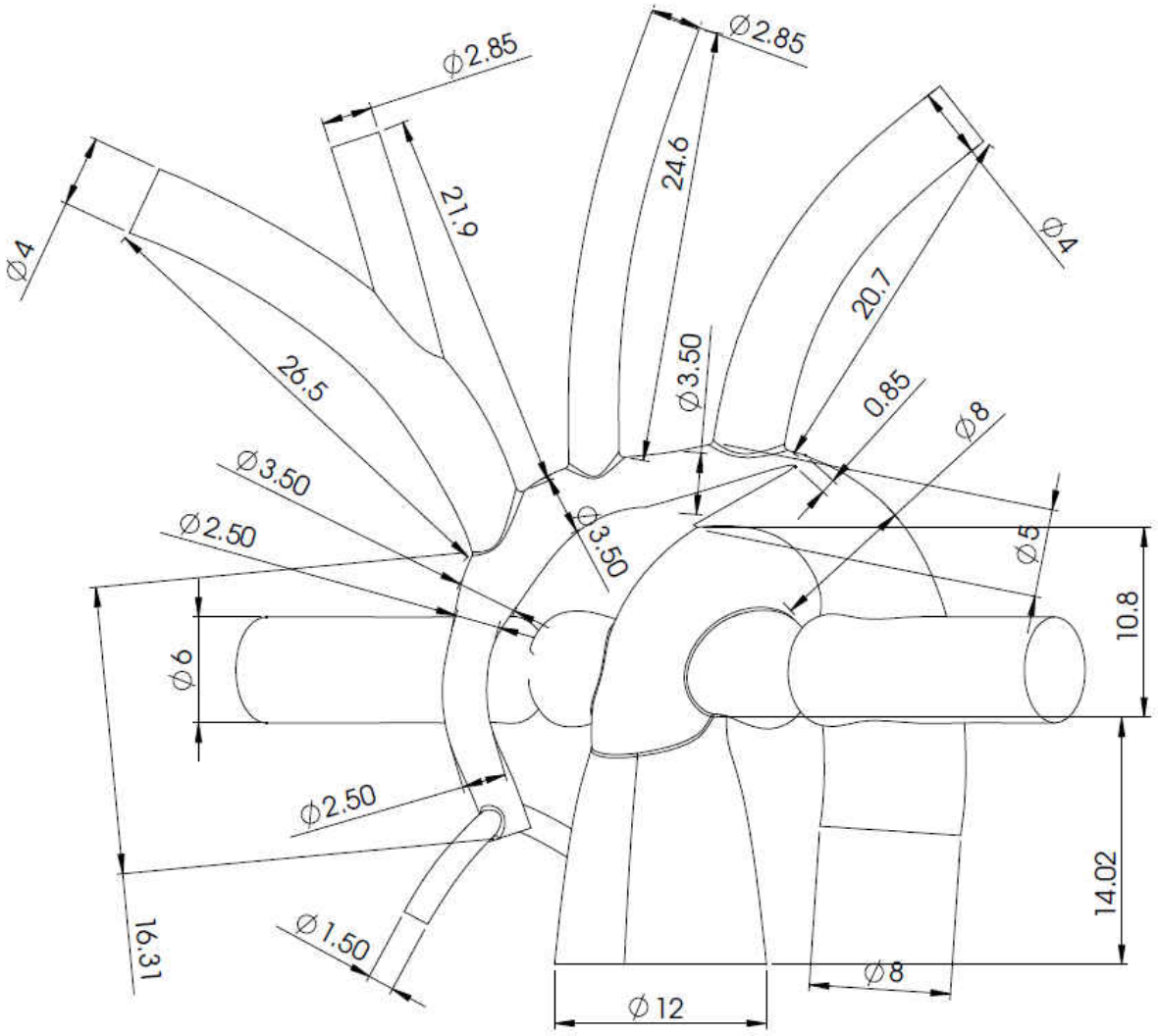

Figure 4.4: Severe Stenosis Case Computational Domain, Dimensions in mm

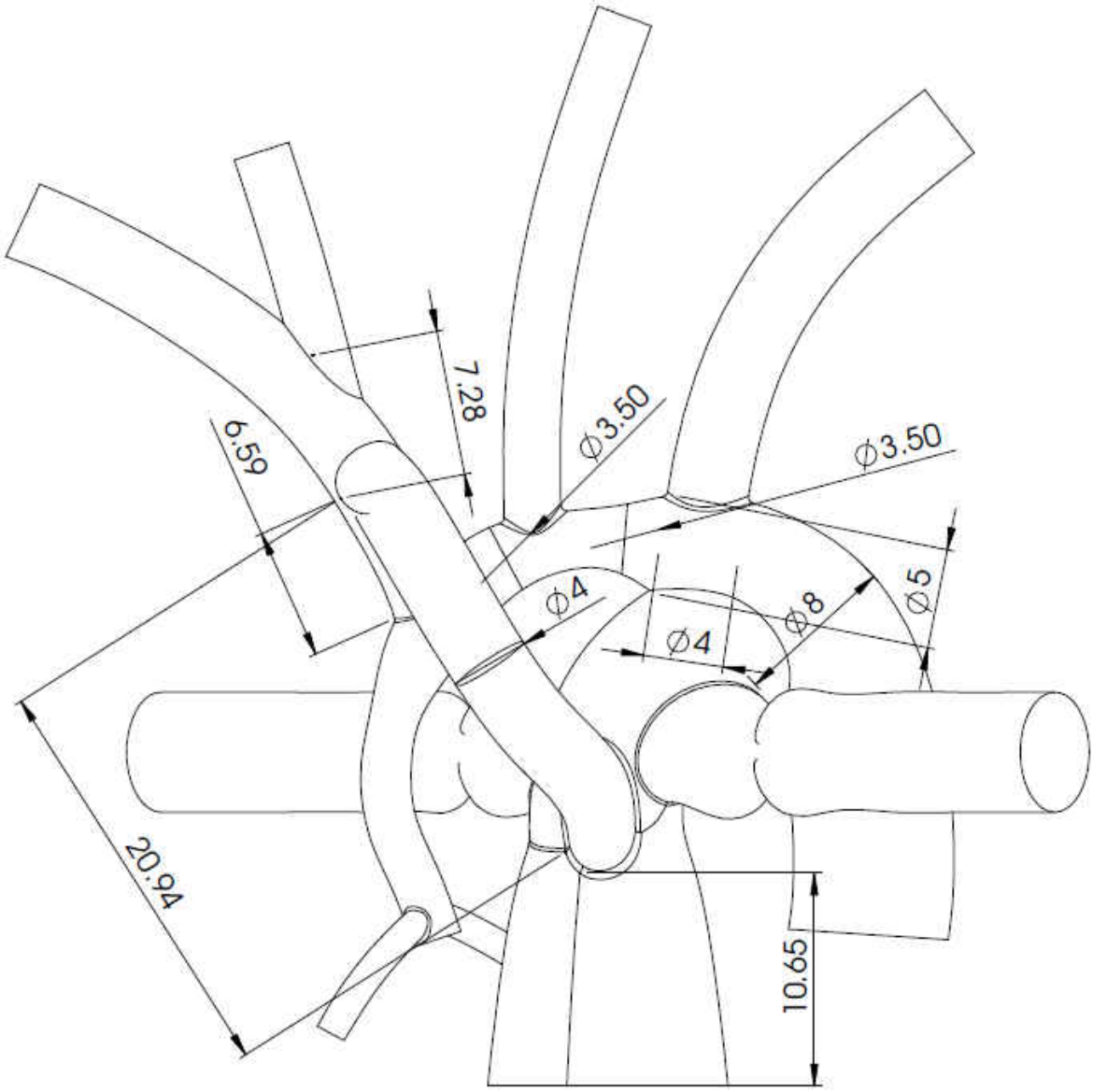

Figure 4.5: Nominal with RBTS Case Computational Domain, Dimensions in mm

4.2 COMPUTATIONAL FLUID DYNAMICS MODEL

4.2.1 FINITE VOLUME MESH

The solid models were imported into Star-CCM+ (CD-adapco, New York, NY), a CFD software that uses the finite volume method to discretize the solution domain. The models were meshed using a hexahedral mesh with fine prism-layer elements near the walls (modeled as rigid) for better boundary layer resolution. Figure 4.6 depicts the overall element distribution in the severe anatomy with RBTS in place. A similar element distribution is obtained for the rest of the models.

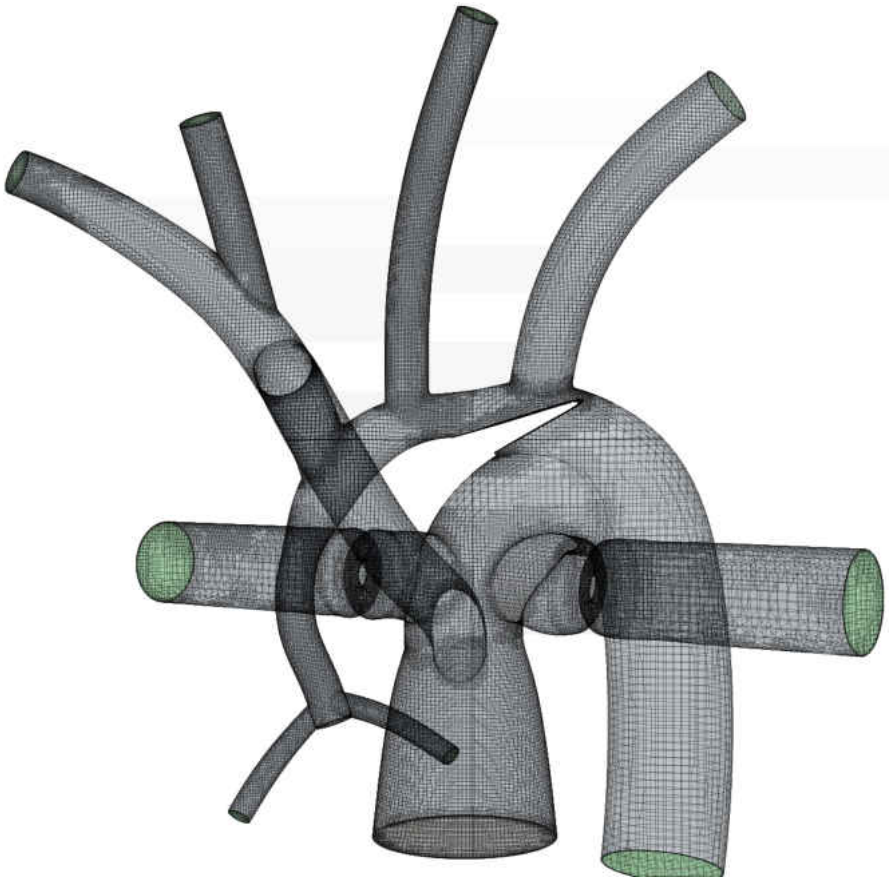

Figure 4.6: Mesh of Computational Domain, Severe with RBTS Anatomy

As seen in the figure above, different areas in the model contain a higher density of elements than others. This is done with the use of size functions that refine the mesh, adding more and smaller elements, in certain areas where sharp changes in the geometry are expected to produce greater flow gradients. In regions where the flow isn't disturbed by abrupt changes in geometry a coarser mesh can be utilized to save computational resources while at the same time maintaining acceptable accuracy. An advantageous meshing feature of the software being utilized is the ability to produce a prism layer of elements, composed of orthogonal prismatic cells, which can more accurately describe the boundary layer and

enable the proper use of turbulence models. Details of the mesh refinement and prism layer are shown in Figure 4.7. The number of elements for the different meshed geometries varied in the range from 1 to 1.2 million.

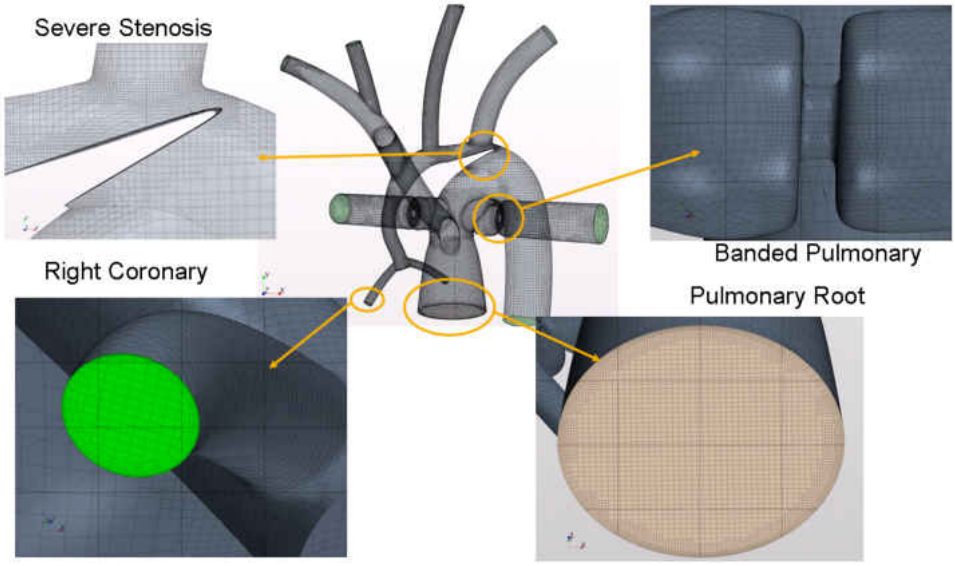

Figure 4.7: Mesh of Computational Domain, Severe with RBTS Anatomy

4.2.2 GOVERNING EQUATIONS

In this particular application blood was modeled as Newtonian and incompressible with a density of 1060 kg/m^3 and a viscosity of 0.004 $Pa-s$. The flow field is resolved by numerically solving the mass and momentum conservation equations, which neglecting gravitational and other body forces and taking into account the aforementioned assumptions, are:

$$\nabla \cdot \vec{V} = 0 \tag{4.1}$$

$$\rho \frac{\partial \vec{V}}{\partial t} + \rho(\vec{V} \cdot \nabla)\vec{V} = -\nabla p + \mu \nabla^2 \vec{V} \tag{4.2}$$

where, $\overrightarrow{V}$ is the flow vector, ρ is the density of the flow, p is the pressure field, and μ is the absolute fluid viscosity. An unsteady, implicit Navier-Stokes equation solver was used over several cardiac cycles, the duration of which is 0.462 seconds. A fully viscous Realizable K-epsilon turbulence model with enhanced wall treatment was adopted. The time step used to advance the solution was 4.62 milliseconds. Unsteady stagnation pressure inlet for the cardiac output and unsteady flow splits were prescribed as boundary conditions derived from the lumped parameter model described in the following section.

4.3 LUMPED PARAMETER MODEL

The lumped parameter (LP) model is used to model the global circulatory system and to provide appropriate boundary conditions to the localized CFD model. The LP model is based on Greenfield-Fry's electrical analogy, where the viscous drag is modeled as a resistor, flow inertia as an inductor, vessel compliance as a capacitor (Figure 4.8). The action of heart valves in the present case is taken to be analogous to ideal diodes, modeled with a Heaviside step function. The Greenfield-Fry solution can be derived from the Navier-Stokes equations expressed in cylindrical coordinates along the direction of the vessel centerline. In differential form this equation can be expressed as:

$$\frac{1}{r}\frac{\partial(r\frac{\partial u}{\partial r})}{\partial r} = \frac{1}{\nu}\frac{du}{dt} + \frac{1}{\mu}\frac{dP}{dx} \tag{4.3}$$

where r is along the radial axis, x is along the direction of the vessel centerline, u is the component of velocity along the x axis, P is the pressure, ν is the kinematic viscosity, $\mu$is the

dynamic viscosity, and t is time. Multiplying the above expression by $2\pi r dr$ and integrating along the radial axis from 0 to R yields, after some algebraic manipulation,

$$\frac{2}{R}\frac{\partial u}{\partial r}|_R = \frac{1}{\nu\pi R^2}\frac{dQ}{dt} + \frac{1}{\mu}\frac{dP}{dx} \tag{4.4}$$

where Q is the volumetric flow rate. For a Newtonian fluid, the shear stress at the wall is proportional to the velocity gradient at the wall,

$$\tau_{wall} = -\mu\frac{\partial u}{\partial r}|_R \tag{4.5}$$

If a further assumption is made that the flow through the vessel is laminar then the Hagen-Poiseuille expression for the shear stress at the wall can be used,

$$\tau_{wall} = \frac{8\mu Q}{2\pi R^3} \tag{4.6}$$

Introducing 4.6 into 4.4 and rearranging to isolate the pressure gradient term yields,

$$-\frac{dP}{dx} = \frac{\rho}{\pi R^2}\frac{dQ}{dt} + \frac{8\mu Q}{\pi R^4} \tag{4.7}$$

The above equation can be expressed as

$$-\frac{dP}{dx} = L_i\frac{dQ}{dt} + R_v Q \tag{4.8}$$

where

$$L_i = c_1\frac{\rho}{\pi R^2} \tag{4.9}$$

$$R_v = c_2\frac{\rho}{\pi R^2} \tag{4.10}$$

The proportionality constants $c_1$and c_2 are introduced from the assumption that in Poiseuille flow the shear stress depends on the flow rate as well as the first derivative of the flow

rate. In the present study L_i and R_v are adjusted iteratively to approach waveforms from catheterization studies. Vessel compliance, analogous to a capacitor, represents the change in volume of the vessel corresponding to a given pressure. This can be expressed as

$$C = \frac{dV}{dP} \tag{4.11}$$

Flow rate to the capacitor can be expressed as

$$Q = \frac{dV}{dt} \tag{4.12}$$

Therefore we can express flow rate as

$$Q = \frac{dV}{dt} = C\frac{dP}{dt} \tag{4.13}$$

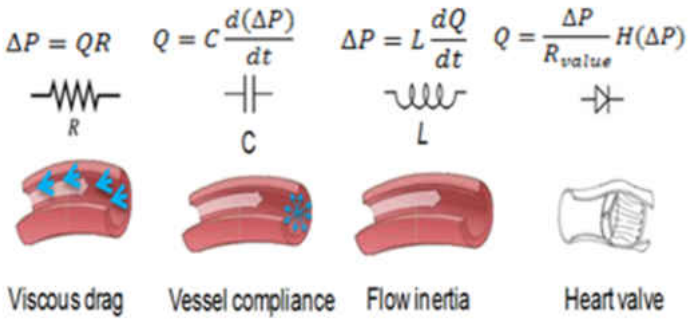

Figure 4.8: Hydraulic-Electrical Analogy Parameters

The ventricle is modeled as a time varying capacitor, the reciprocal of which is called elastance. This elastance provides the pulsatile nature of the cardiac output and is the driving function of the circuit. It provides the relationship for ventricular pressure and volume at a given point during the cardiac cycle. Mathematically it is expressed as[15] :

$$E(t) = \frac{VP(t)}{VV(t) - V_0} \tag{4.14}$$

where $E(t)$ is the time varying elastance, $VP(t)$ is the ventricular pressure, $VV(t)$ is the ventricular volume, and V_0 is the theoretical volume of the ventricle at zero pressure. Numerous formulations have been developed to obtain $E(t)$, in the present study a formulation similar to that employed by Simaan et. al.[16] was chosen, where

$$E(t) = (E_{max} - E_{min}) \cdot E_n(t_n) + E_{min} \tag{4.15}$$

The therm $E_n(t_n)$ is the "double hill" function[17]:

$$E_n(t_n) = \left[\frac{\left(\frac{t_n}{0.303}\right)^{1.32}}{1 + \left(\frac{t_n}{0.303}\right)}\right]\left[\frac{1}{1 + \left(\frac{t_n}{0.508}\right)^{21.9}}\right] \tag{4.16}$$

where $E_n(t_n)$ is the normalized time varying elastance, $t_n = \frac{t}{t_c}$,$t_c = \frac{60}{HR}$ the cardiac cycle period, and HR is the heart rate (130 beats per minute in this case). The values for E_{max}, E_{min}, and the exponential coefficients were tuned iteratively to provide a physiologically correct cardiac output. Figure 4.14 depicts the elastance function over one cardiac cycle.

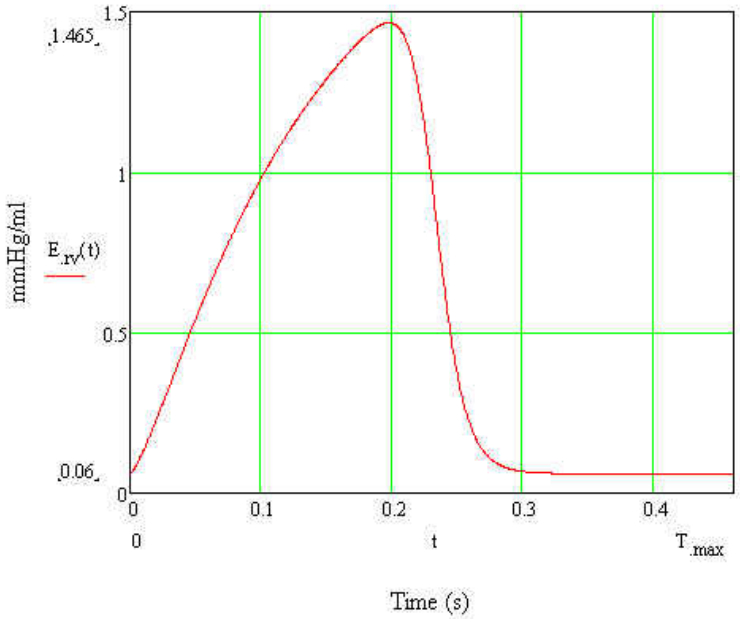

Figure 4.9: Elastance Function

The different vascular beds are modeled as RLC compartments (Figure 4.10) with the whole circuit tied together in a closed loop representation of physical anatomy. Each terminal load is divided into two compartments, one simulating the arterial bed and the other the venous bed. This was necessary in order to impose the appropriate boundary conditions to the CFD model. The resulting circuit (Figure 4.11) contains 32 state variables and the ensuing system of ordinary differential equations is solved using a 4th Order Runge-Kutta integrator with adaptive time step.

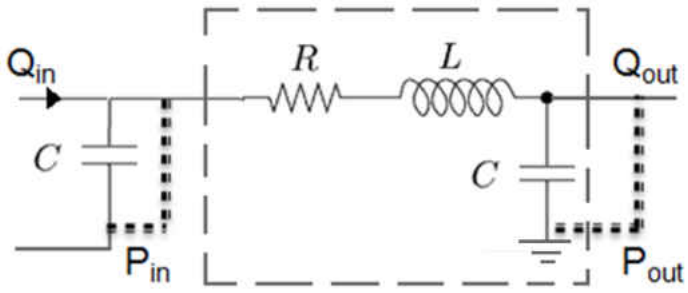

Figure 4.10: Electrical Compartment Analogous to Vascular Bed

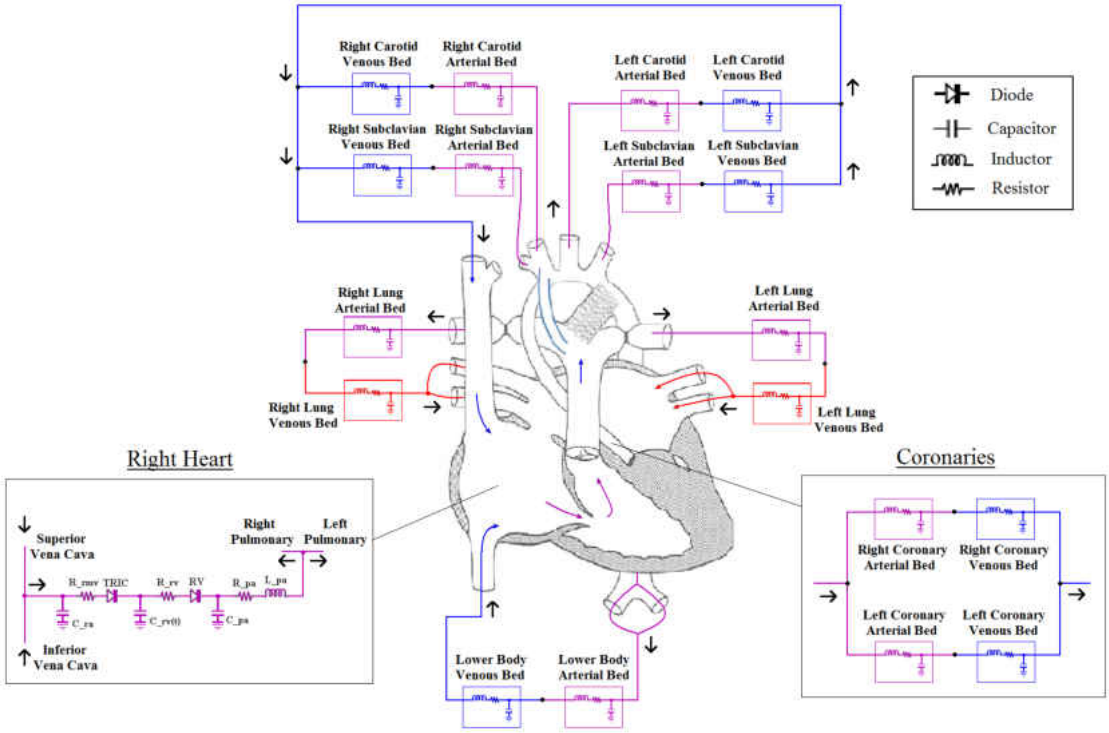

Figure 4.11: Peripheral Vasculature Circuit Drawing

The coupling of the two models is done in the following manner: 1) The initial circuit is tuned to produce target flows and pressure waveforms obtained from catheter studies and surgeon's criteria, 2) Flow splits and inlet boundary conditions are imposed to the CFD

from the circuit, 3) CFD simulation is carried out to obtain pressure waveforms, 4) The CFD equivalent parameters within the circuit are modified to match those derived from the CFD solution, 5) Impose new flow splits from circuit to CFD, 6) Iterate until convergence (Figure 4.12). Once this iterative process is complete, the CFD simulation is run for 3 cardiac cycles and post-processing is performed.

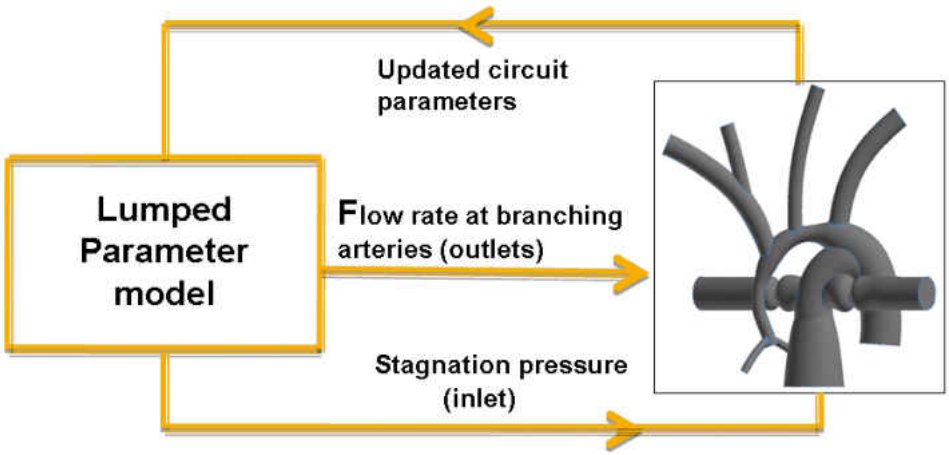

Figure 4.12: Multiscale Model Coupling Scheme

CHAPTER 5
RESULTS

5.1 FLOW QUANTITIES

As stated earlier, there are four configurations that were studied: a nominal case where no stenosis or RBTS are present, a nominal case with the RBTS in place, a severe stenosed case without RBTS, and a severe stenosed case with the RBTS in place. The flow and pressure waveforms obtained for the different configurations at the boundaries of the CFD model are shown in Figures 5.1 through 5.11. A summary of cardiac output, the relative flow rates through the shunt and branching arteries, and the ratio of pulmonary to systemic circulation is presented in Table 5.1. Table 5.2 quantifies the percent change in flow relative to the nominal case. As expected, there is a significant reduction in both pressure and net flow rate through the arteries of interest when the severe stenosis is present. The performance of the RBTS shunt is highly satisfactory, returning the pressure and flow rate values to near stenosis-free levels. Notice there are no adverse effects when implementing the RBTS without stenosis, on the contrary, there is a slight increase in flow rate to all arterial beds. This supports the idea of implanting the shunt as a preventative measure in case stenosis develops with time after the initial procedure, reducing or eliminating the need for re-intervention. Of concern to surgeons was the possible "siphoning" effect that might occur during diastole, in which the lower pressure in the pulmonary circulation creates flow reversal and could

be exacerbated by the addition of the RBTS [18]. As seen in Figures 5.1and 5.8, there is a slightly higher amount of reverse flow with the RBTS in place with the Nominal configuration but this is offset by higher peak flow. The same behavior is not exhibited in the other configurations.

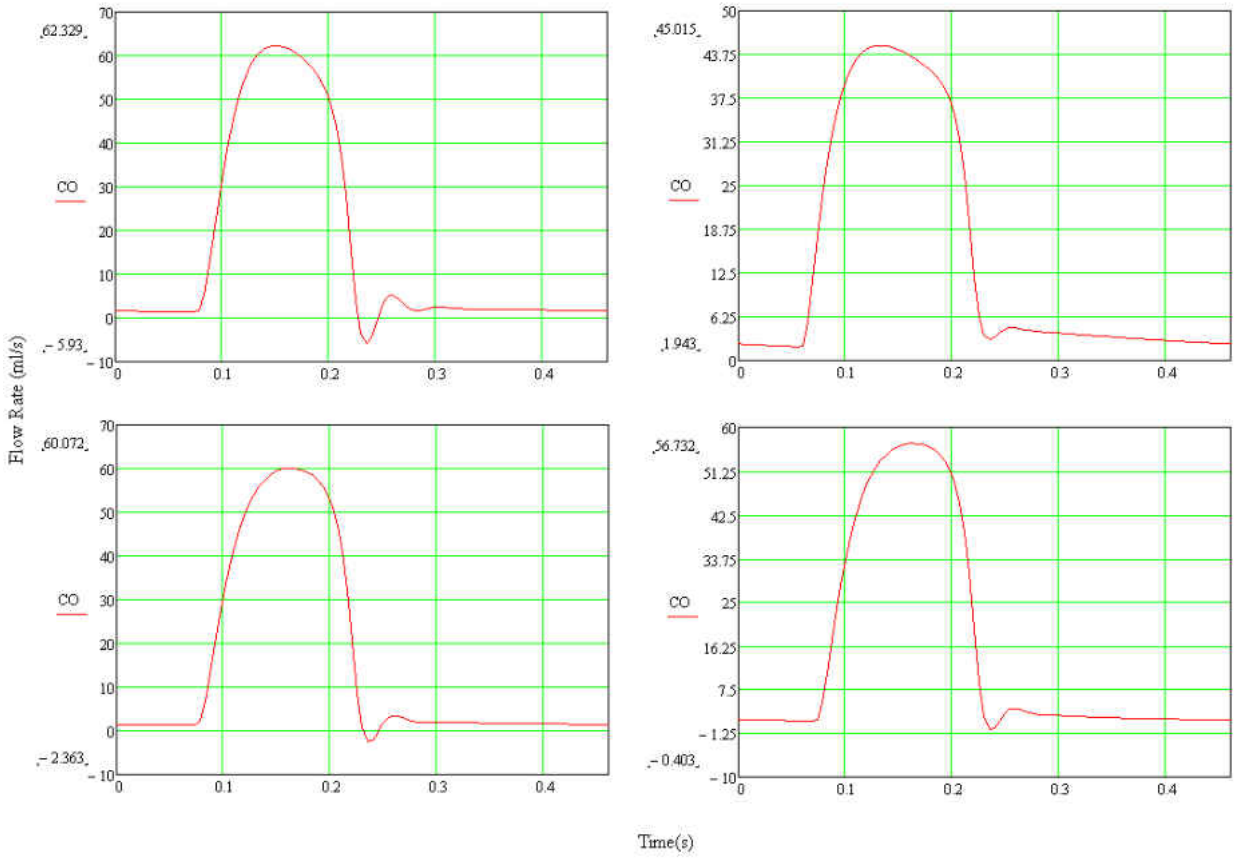

Figure 5.1: Cardiac Output of All Configurations, Nominal (Top Left), Severe (Top Right), Nominal with RBTS (Bottom Left), Severe with RBTS (Bottom Right)

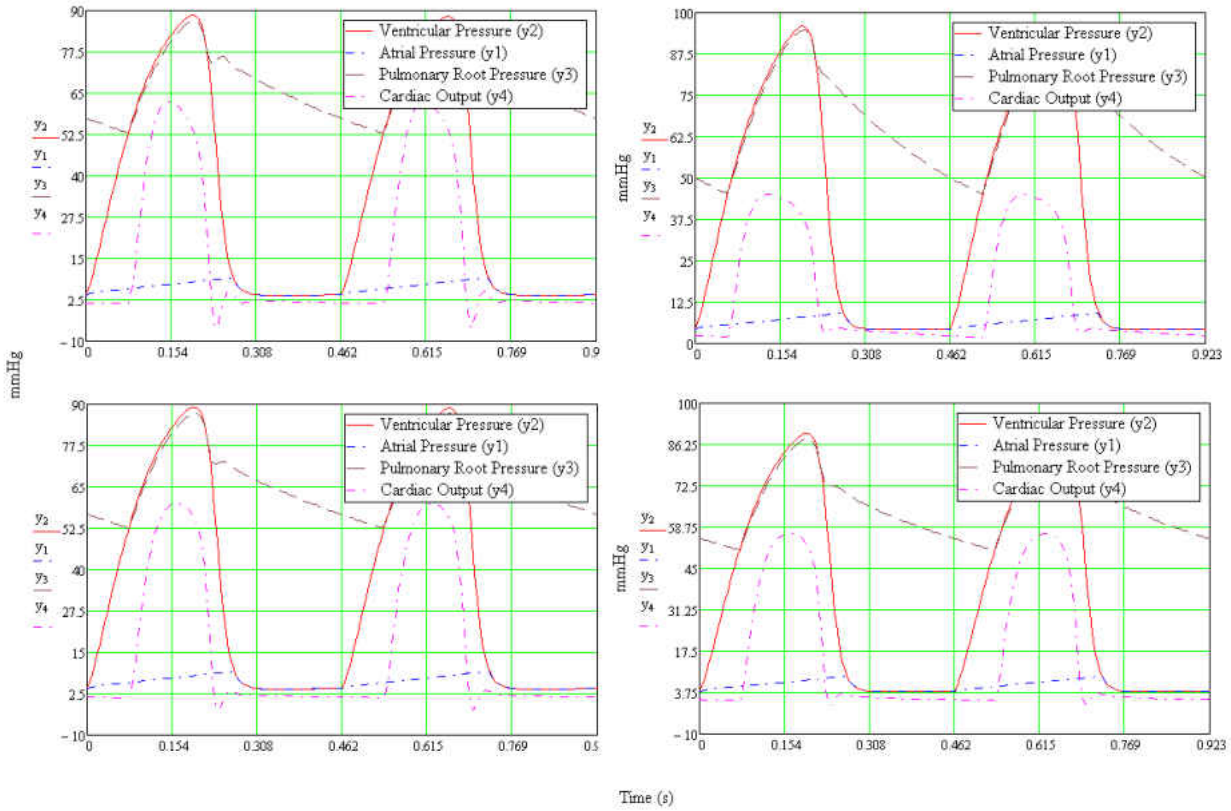

Figure 5.2: Cardiac Pressure with Cardiac Output Superimposed of All Configurations Over Two Cycles, Nominal (Top Left), Severe (Top Right), Nominal with RBTS (Bottom Left), Severe with RBTS (Bottom Right)

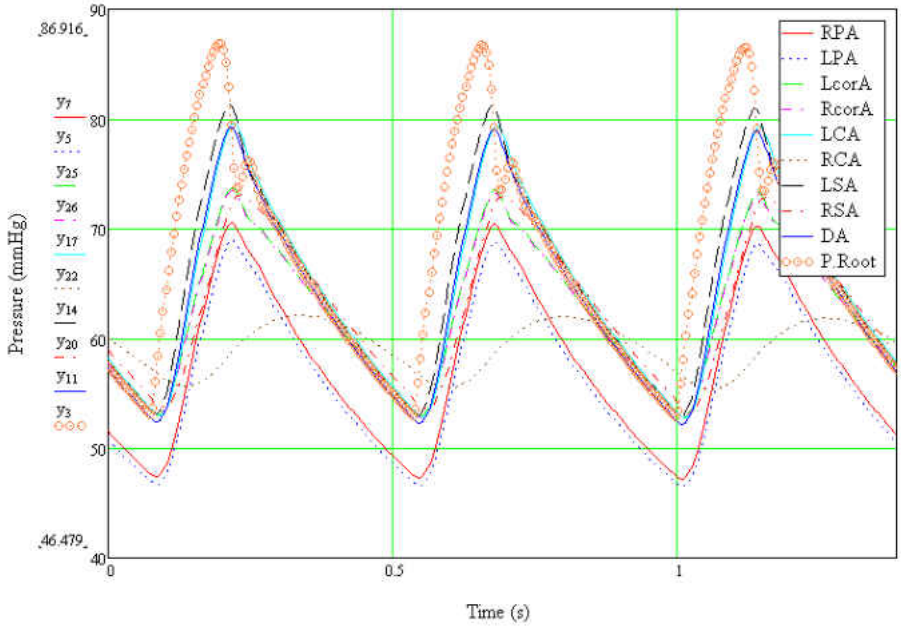

Figure 5.3: Composite of Arterial Pressure at Interfaces, Nominal Configuration

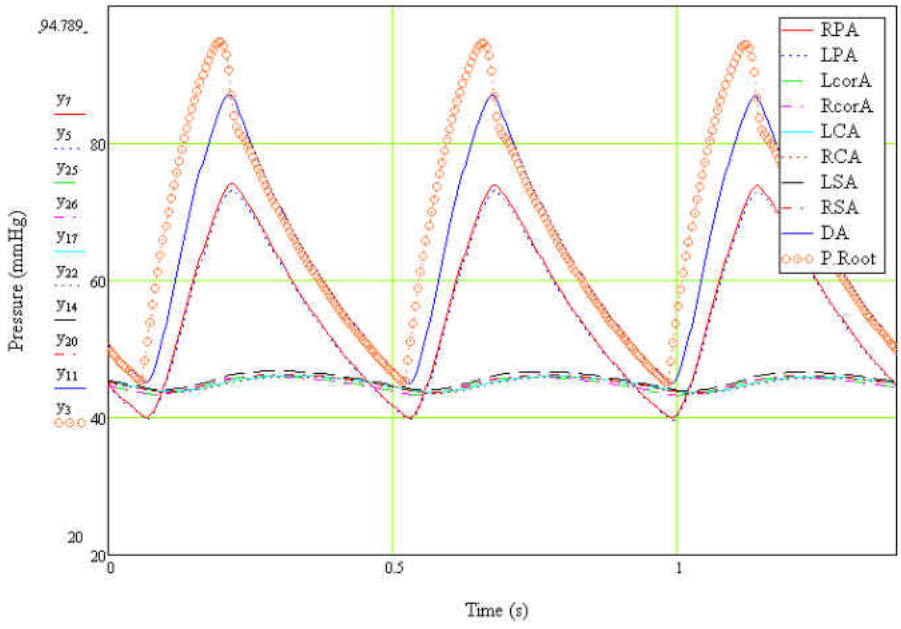

Figure 5.4: Composite of Arterial Pressure at Interfaces, Severe Configuration

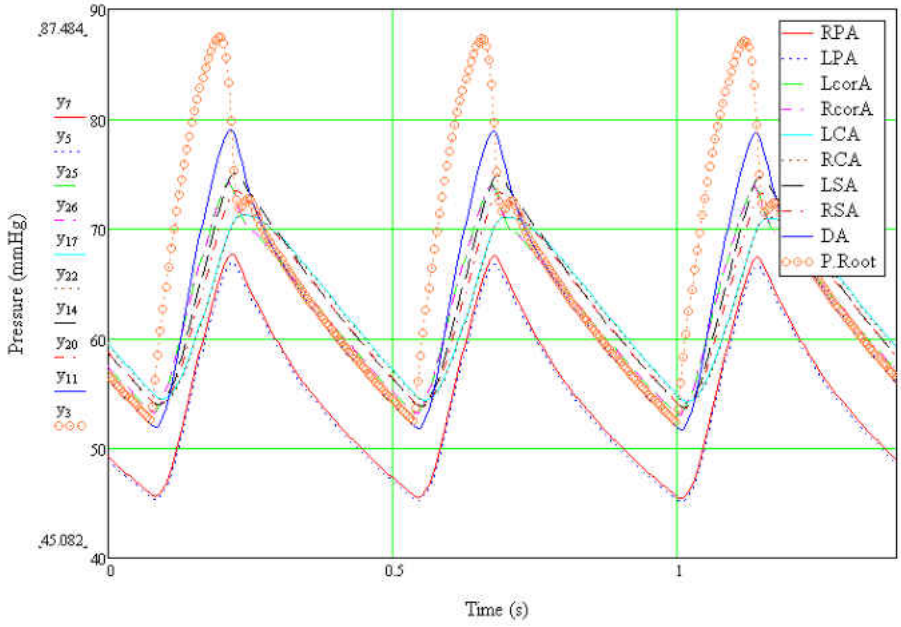

Figure 5.5: Composite of Arterial Pressure at Interfaces, Nominal with RBTS Configuration

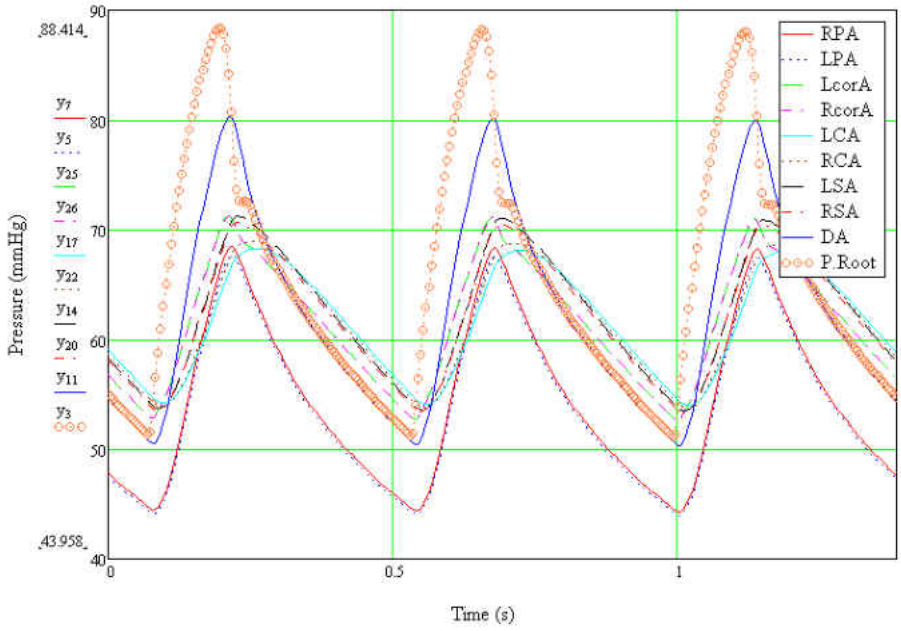

Figure 5.6: Composite of Arterial Pressure at Interfaces, Severe with RBTS Configuration

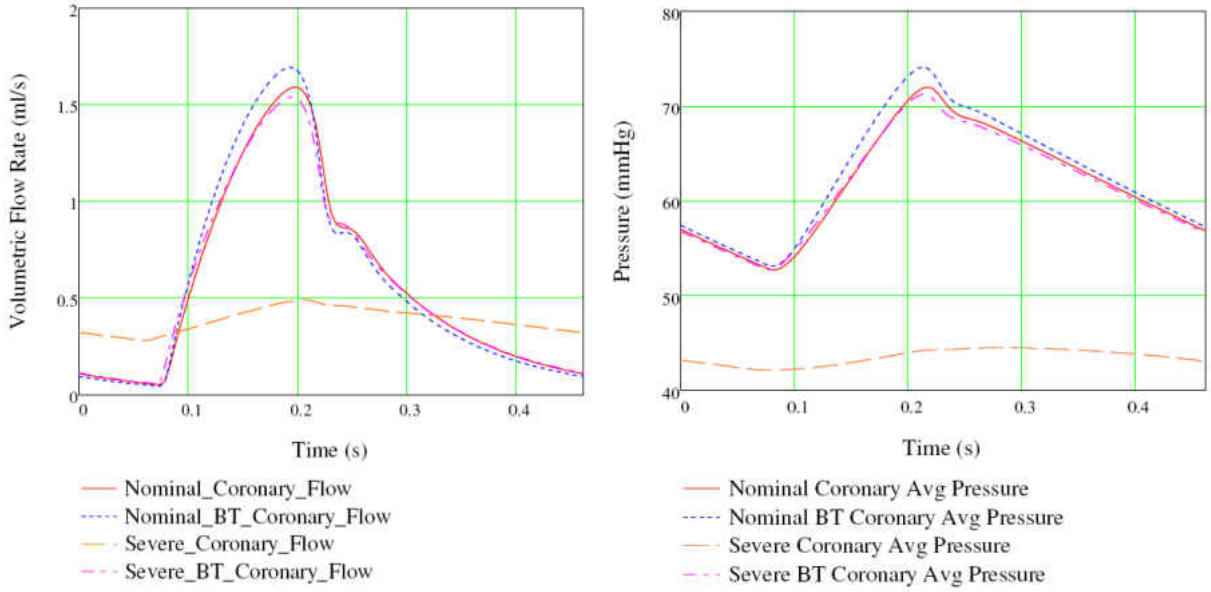

Figure 5.7: Pressure and Flow Rate Waveforms at Coronary Artery Boundaries

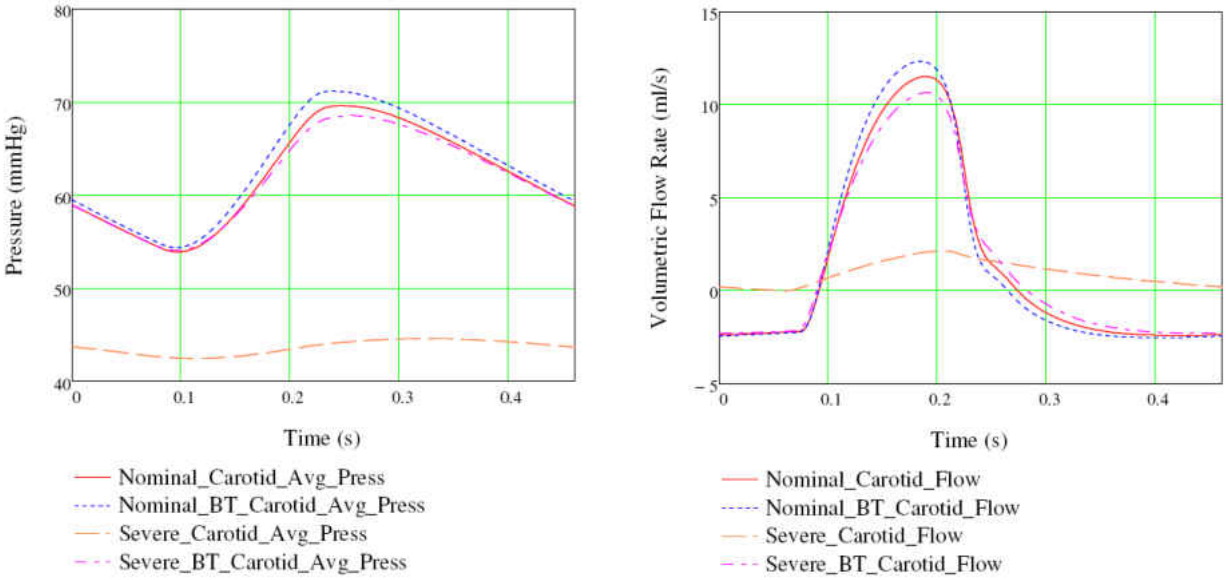

Figure 5.8: Pressure and Flow Rate Waveforms at Carotid Artery Boundaries

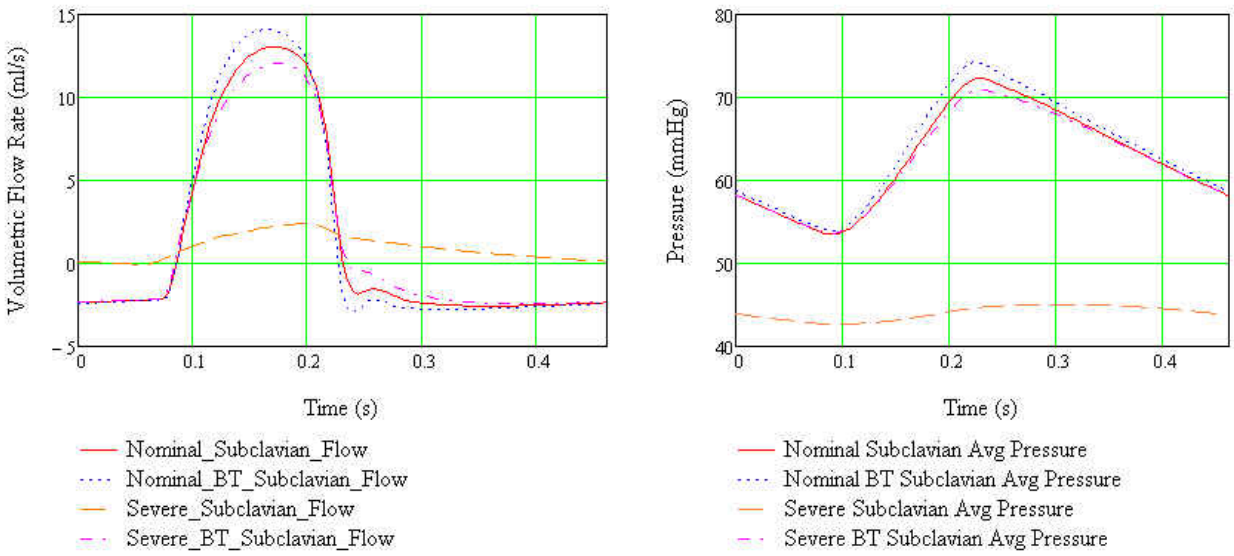

Figure 5.9: Pressure and Flow Rate Waveforms at Subclavian Artery Boundaries

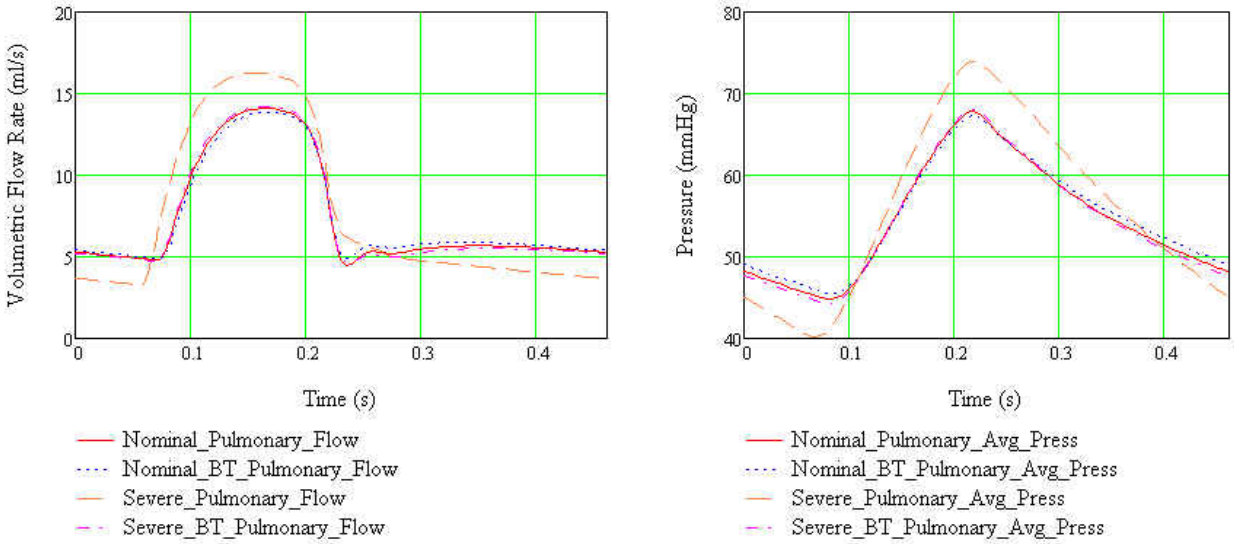

Figure 5.10: Pressure and Flow Rate Waveforms at Pulmonary Artery Boundaries

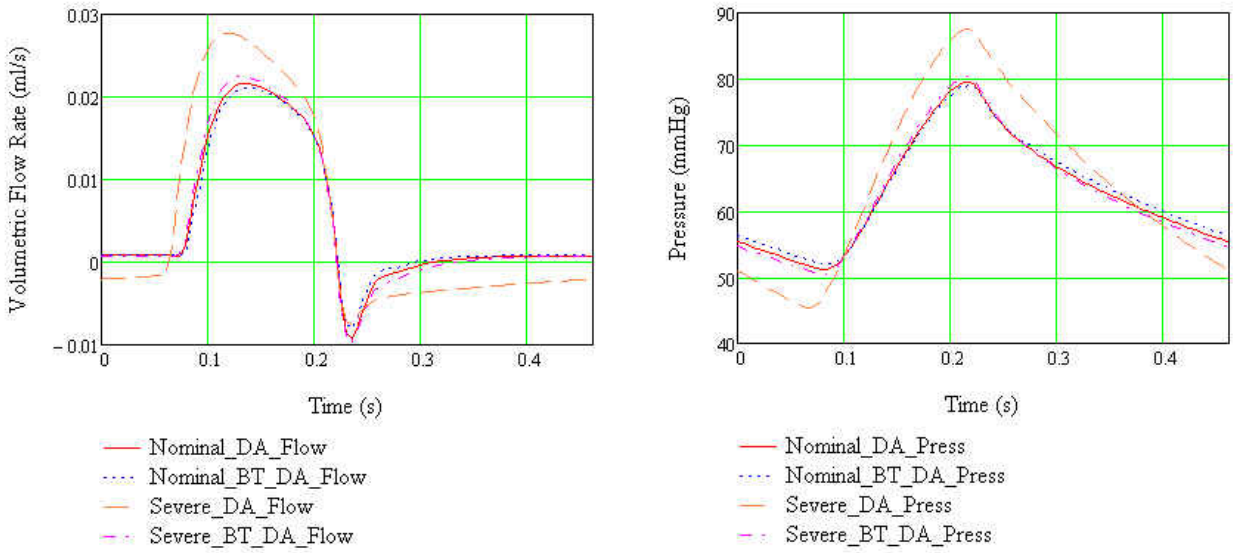

Figure 5.11: Pressure and Flow Rate Waveforms at the Descending Aorta Boundary

Table 5.1: Flow Rate Summary for All Anatomical Configurations

	Cardiac Output (ml/min)	Flow Rate as Percentage of Cardiac Output										
		DA	LCA	LcorA	LPA	LSA	RCA	RcorA	RPA	RSA	Shunt	Qs/Qp
Nominal	2005	29.64	4.55	1.87	24.06	4.62	4.53	1.87	24.29	4.56	NA	1.068
Nominal_BT-Shunt	2025	29.58	4.57	1.89	24.01	4.65	4.57	1.89	24.23	4.60	9.06	1.073
Severe	1902	31.96	3.39	1.37	25.72	3.44	3.38	1.37	25.96	3.40	NA	0.935
Severe_BT-Shunt	2001	29.72	4.52	1.87	24.06	4.59	4.53	1.87	24.28	4.56	20.97	1.068

Table 5.2: Flow Rate Difference with Respect to Nominal Configuration

	Percentage Increase Over Nominal										
	Cardiac Output	DA	LCA	LcorA	LPA	LSA	RCA	RcorA	RPA	RSA	Qs/Qp
Nominal_BT-Shunt	0.97	0.77	1.50	1.76	0.73	1.50	1.77	1.76	0.73	1.79	0.41
Severe	-5.15	2.28	-29.33	-30.45	1.39	-29.37	-29.28	-30.45	1.39	-29.30	-12.48
Severe_BT-Shunt	-0.21	0.06	-0.93	-0.24	-0.22	-0.96	-0.30	-0.24	-0.22	-0.32	0.02

5.2 FLOW VISUALIZATION

A major advantage of the multiscale model is its ability to provide detailed local hemodynamics. Figures 5.14 through 5.31 show pressure, velocity, velocity vector, and streamline contour plots among the different anatomical configurations at selected points during the cardiac cycle. Figure 5.12 shows the location of the points chosen with the use of nominal cardiac output plot (flow at the root of the pulmonary artery).

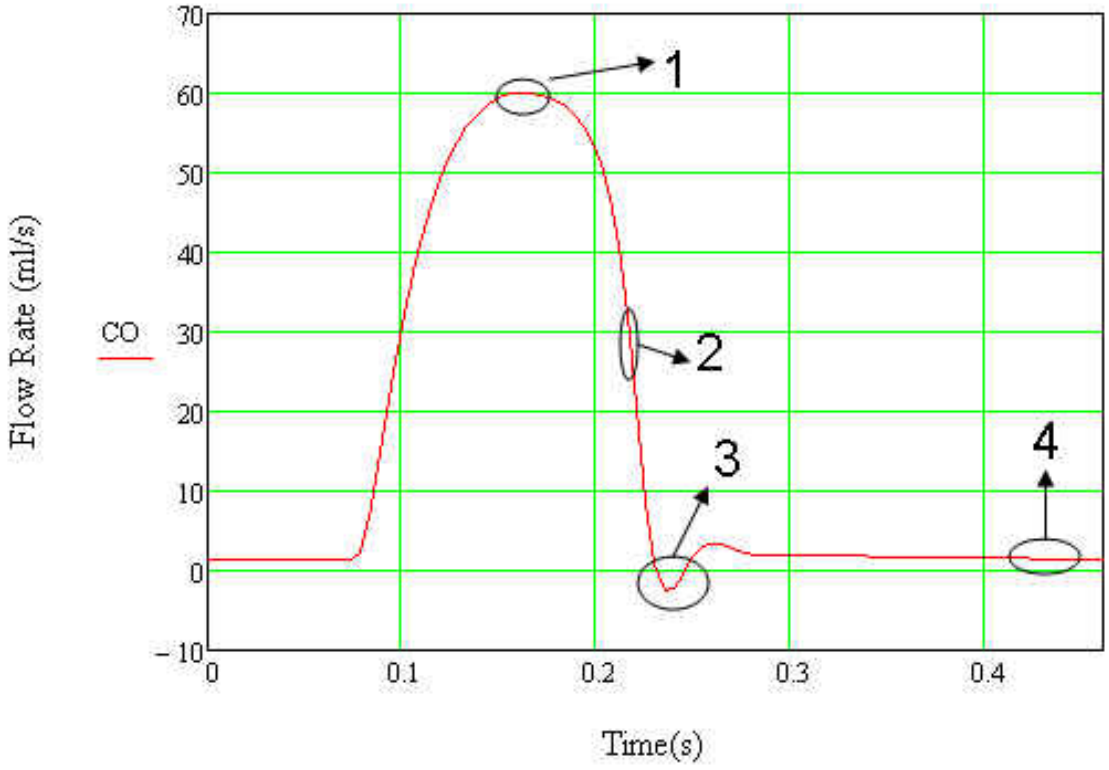

Figure 5.12: Visualization Locations Relative to Cardiac Cycle

The numbered regions in the above figures correspond to the following:

1. Peak pulmonary root flow and ventricular pressure during the rapid ejection phase.
2. Median pulmonary root flow and ventricular pressure during the reduced ejection phase.
3. Brief period of limited reverse flow after aortic valve closure corresponding to low ventricular pressure during the isovolumic relaxation phase.
4. Period of low or no ejection corresponding to low ventricular pressure during the reduced ventricular filling phase.

Figure 5.13 shows the location of plots corresponding to each point during the cardiac cycle in subsequent figures.

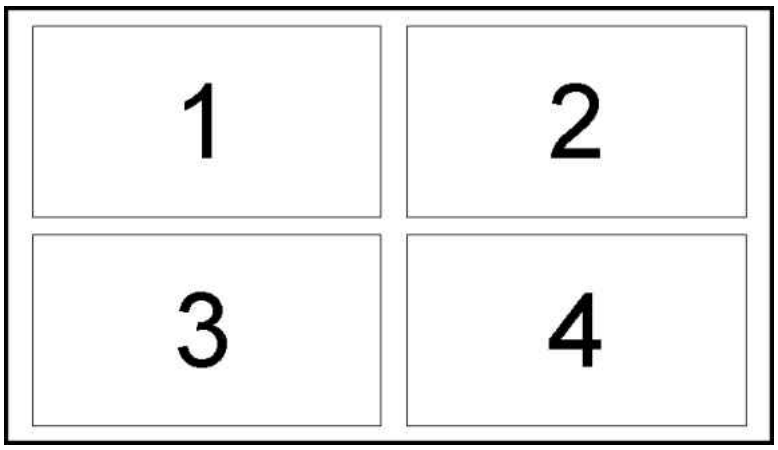

Figure 5.13: Plot Location Relative to Cardiac Cycle Phase

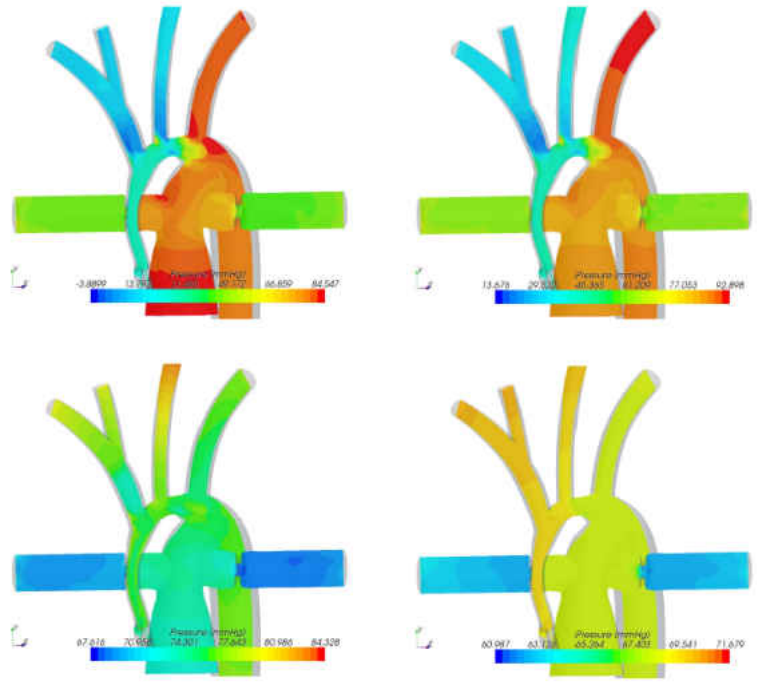

Figure 5.14: Pressure Contour Plot of Nominal Configuration

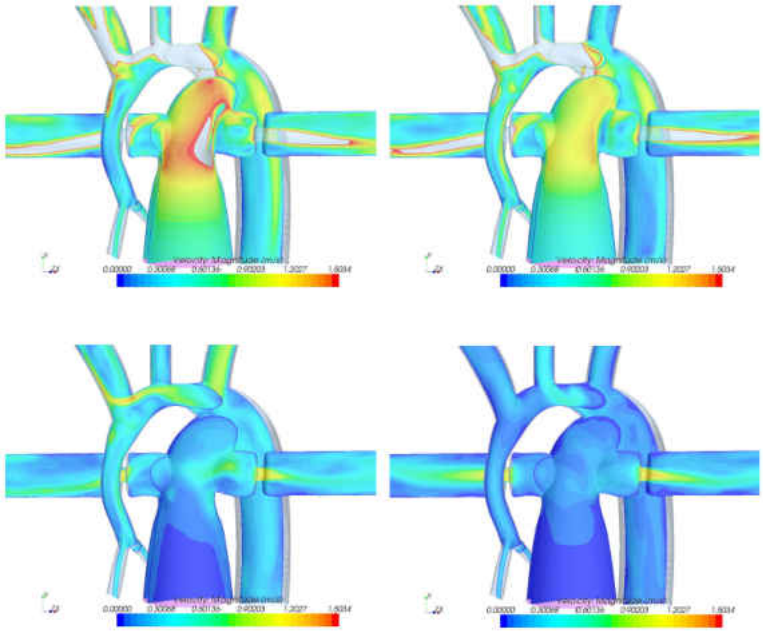

Figure 5.15: Velocity Contour Plot of Nominal Configuration

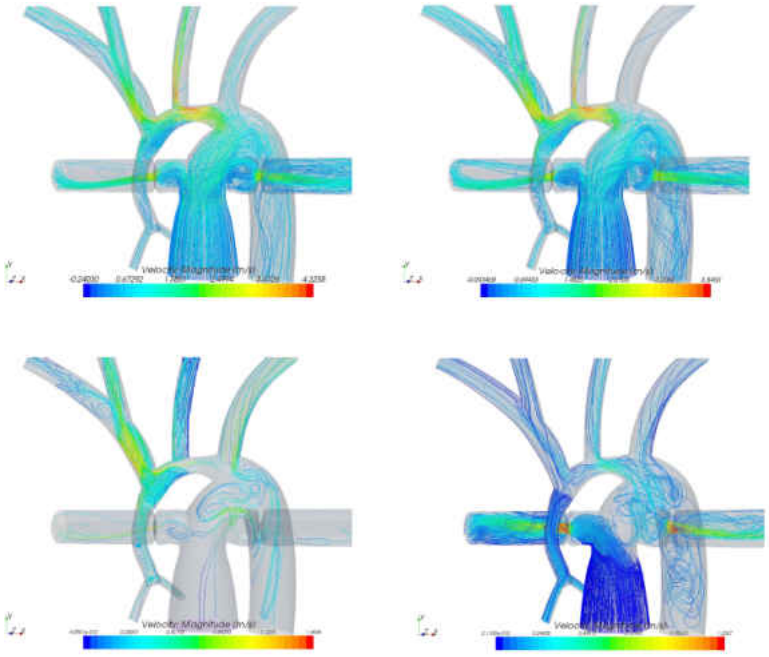

Figure 5.16: Streamlines Colored by Velocity of Nominal Configuration

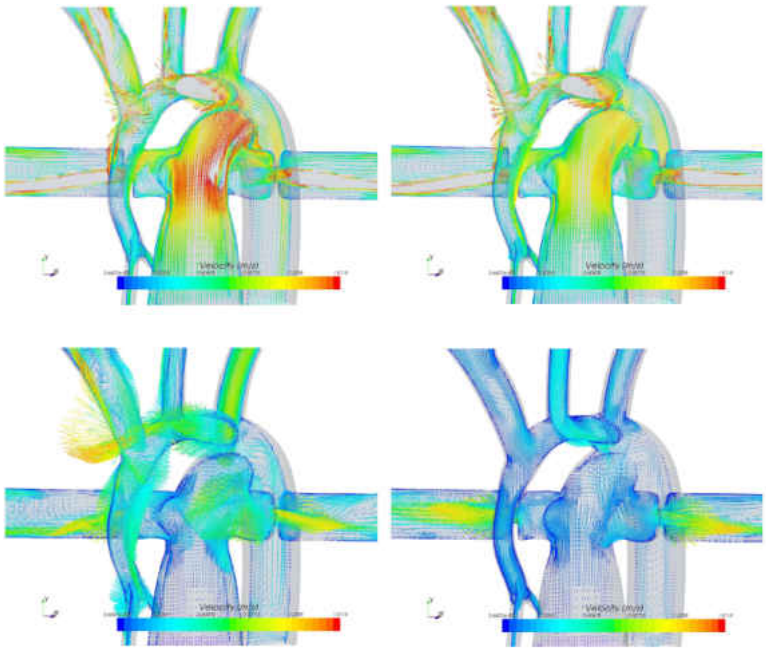

Figure 5.17: Velocity Vector Plot of Nominal Configuration

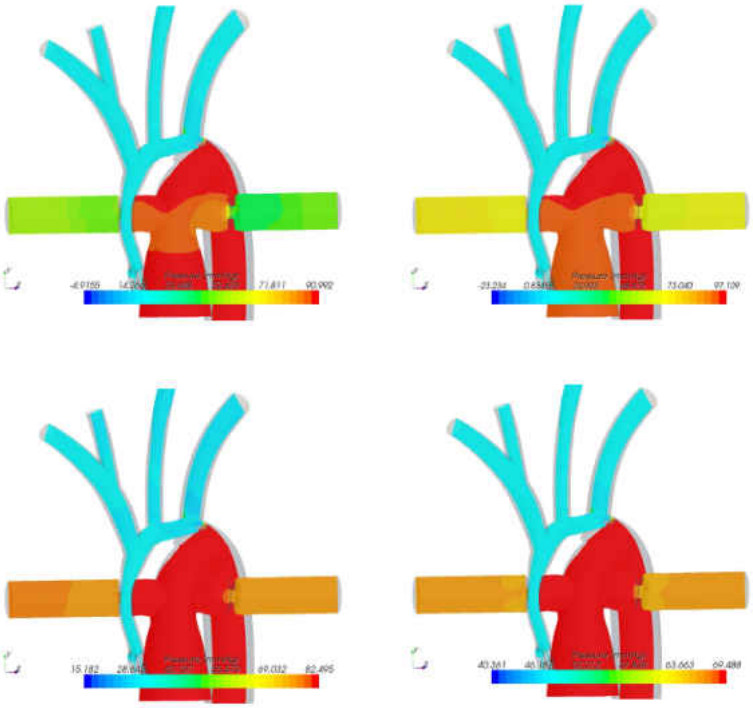

Figure 5.18: Pressure Contour Plot of Severe Stenosis Configuration

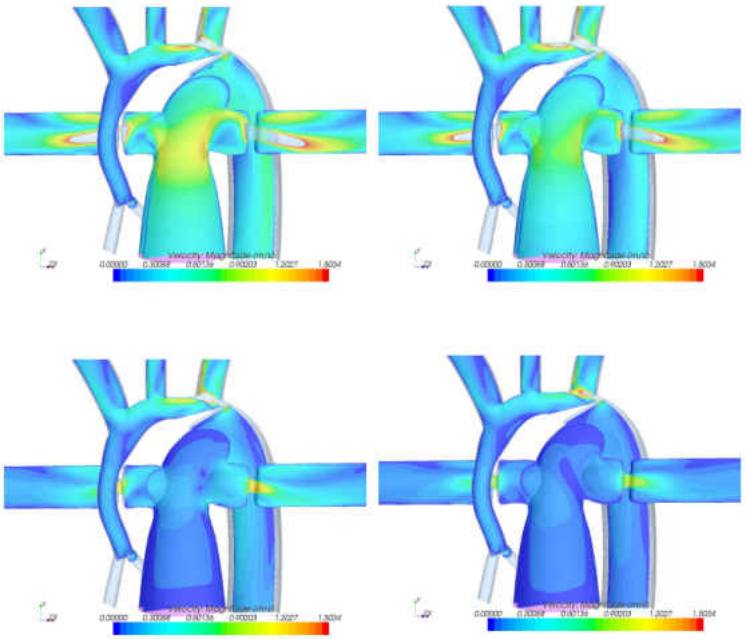

Figure 5.19: Velocity Contour Plot of Severe Stenosis Configuration

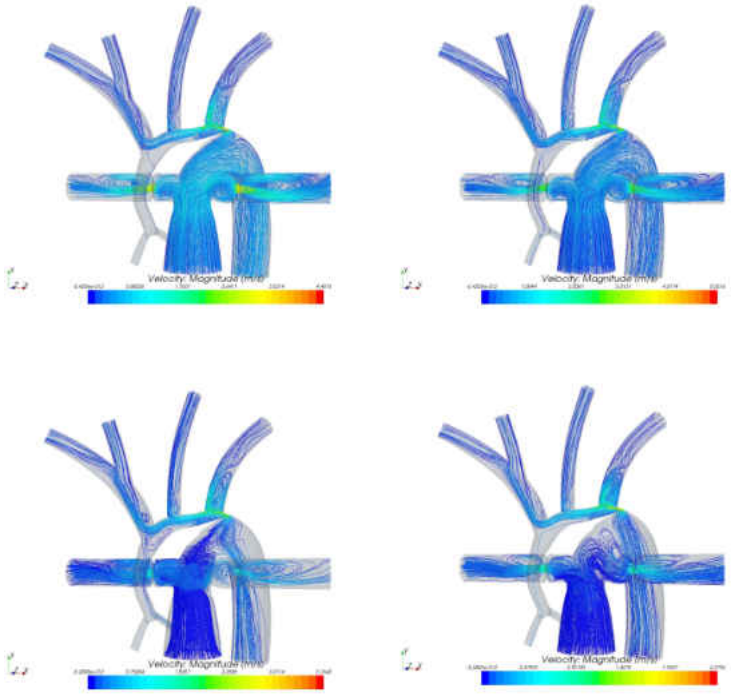

Figure 5.20: Streamlines Colored by Velocity of Severe Stenosis Configuration

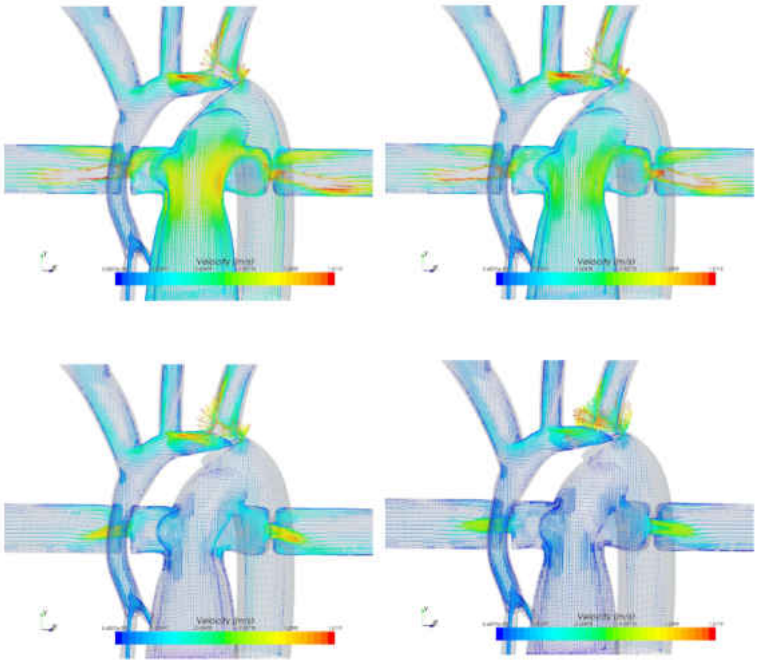

Figure 5.21: Velocity Vector Plot of Severe Stenosis Configuration

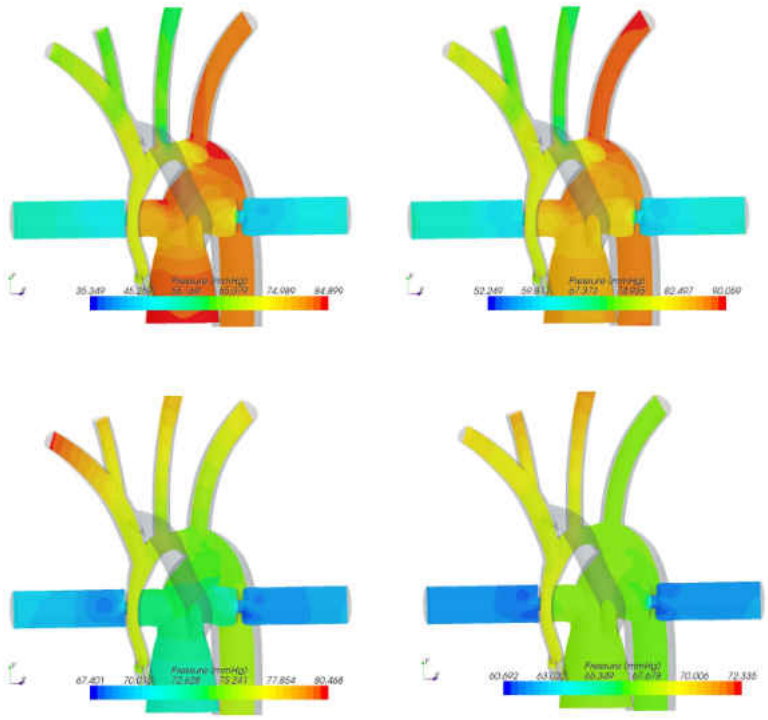

Figure 5.22: Pressure Contour Plot of Nominal with RBTS Configuration

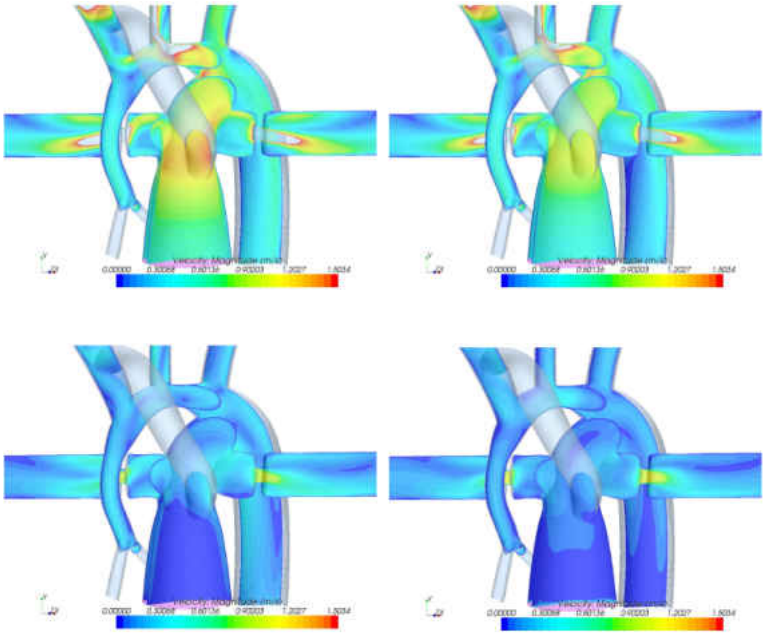

Figure 5.23: Velocity Contour Plot of Nominal with RBTS Configuration

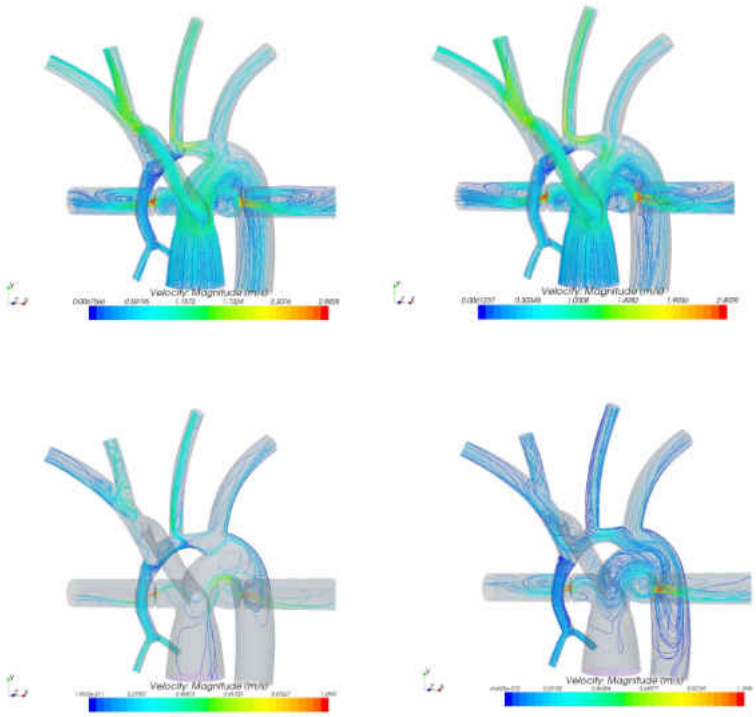

Figure 5.24: Streamlines Colored by Velocity of Nominal with RBTS Configuration

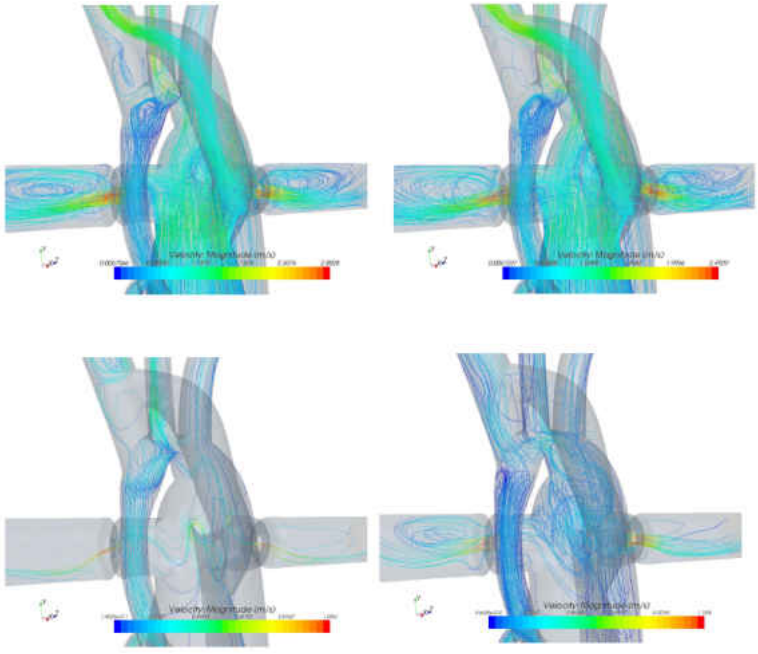

Figure 5.25: Streamlines Colored by Velocity of Nominal with RBTS Configuration

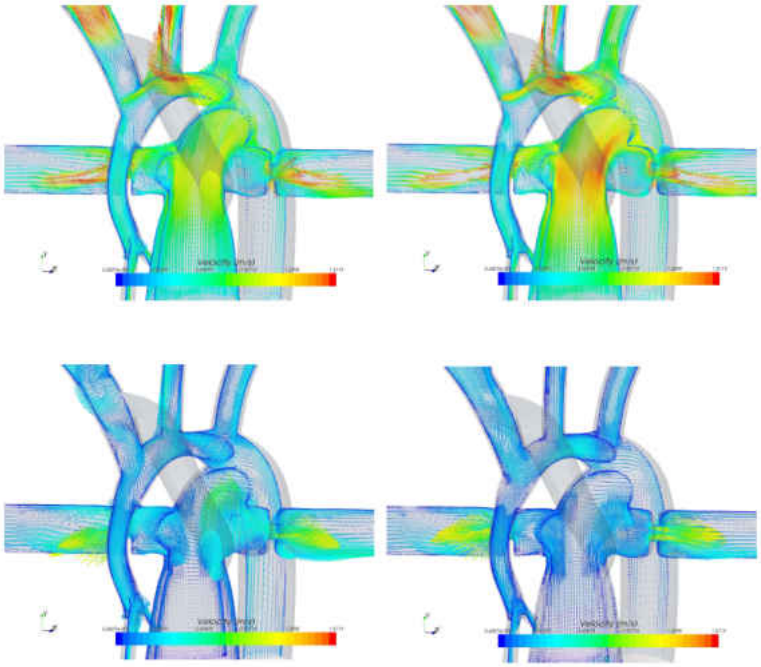

Figure 5.26: Velocity Vector Plot of Nominal with RBTS Configuration

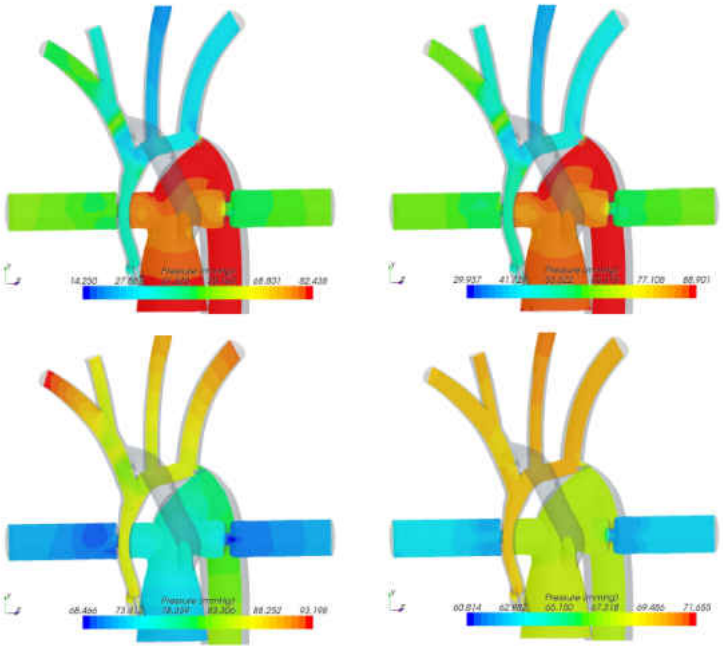

Figure 5.27: Pressure Contour Plot of Severe Stenosis with RBTS Configuration

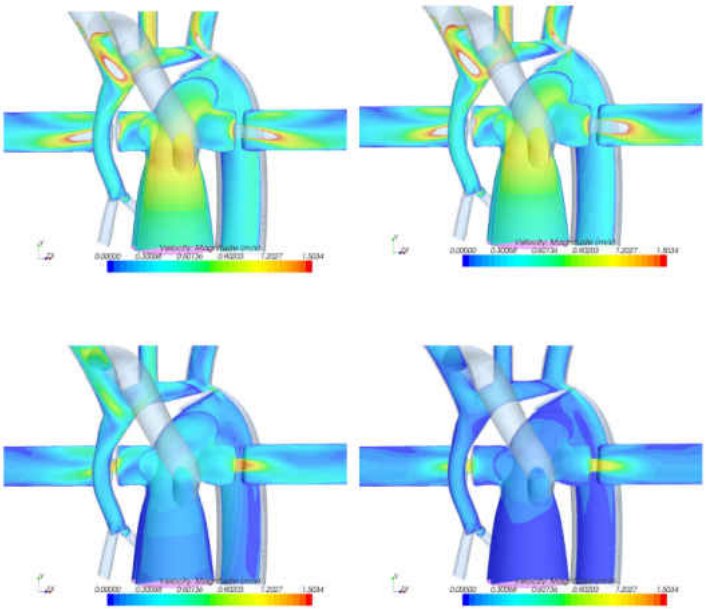

Figure 5.28: Velocity Contour Plot of Severe Stenosis with RBTS Configuration

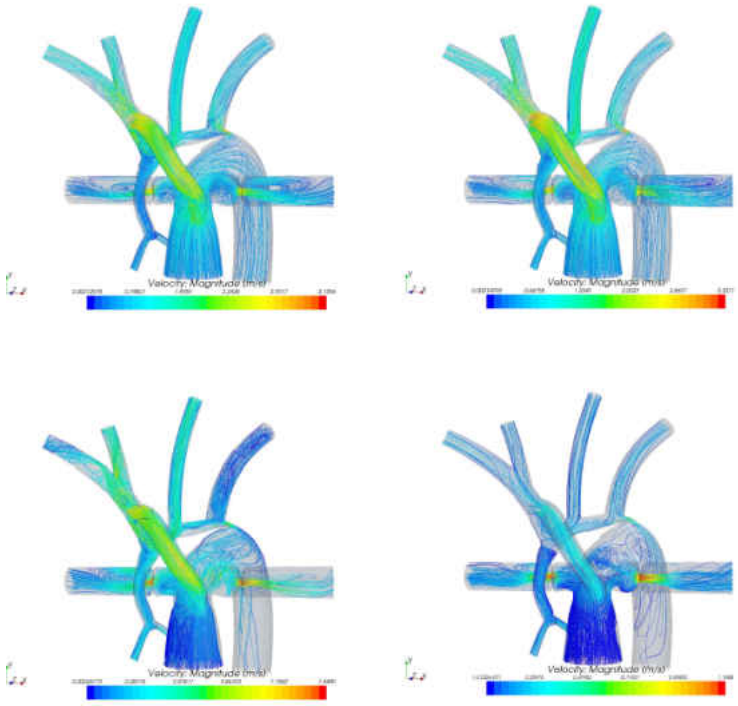

Figure 5.29: Streamlines Colored by Velocity of Severe Stenosis with RBTS Configuration

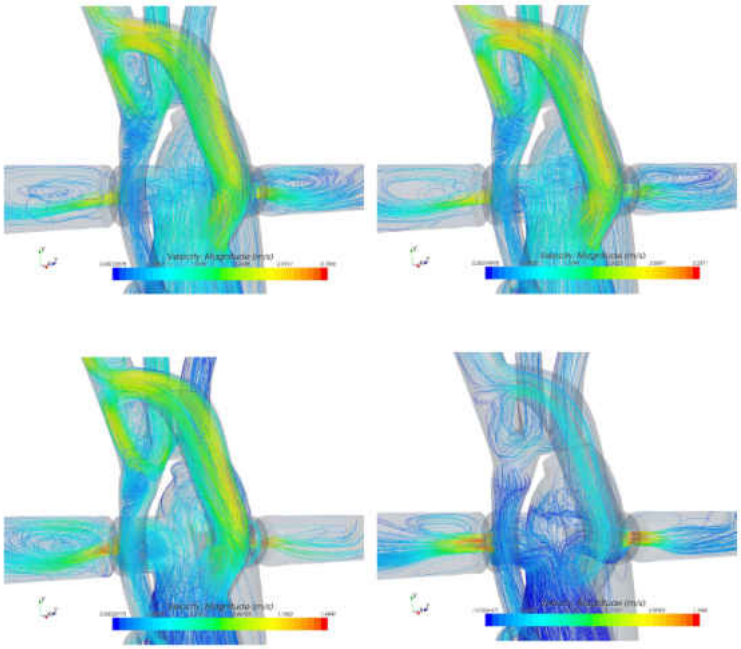

Figure 5.30: Streamlines Colored by Velocity of Severe Stenosis with RBTS Configuration

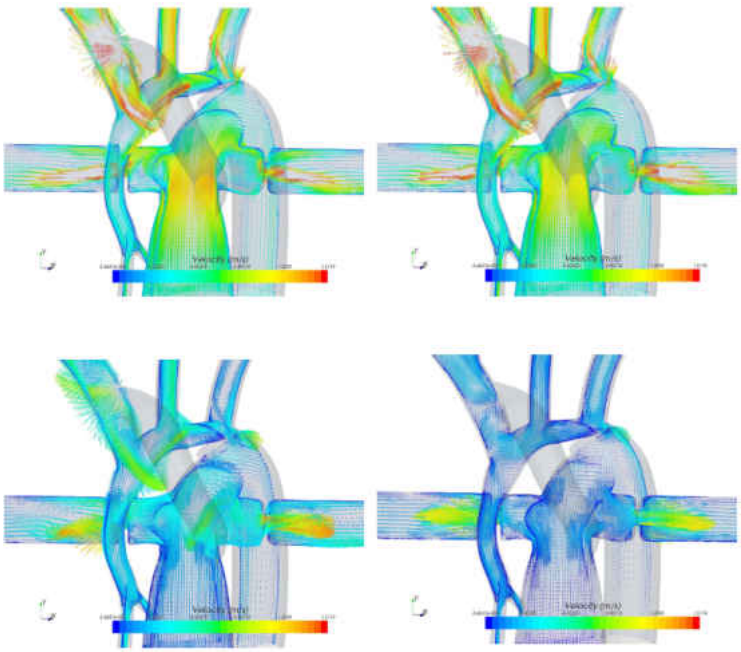

Figure 5.31: Velocity Vector Plot of Severe Stenosis with RBTS Configuration

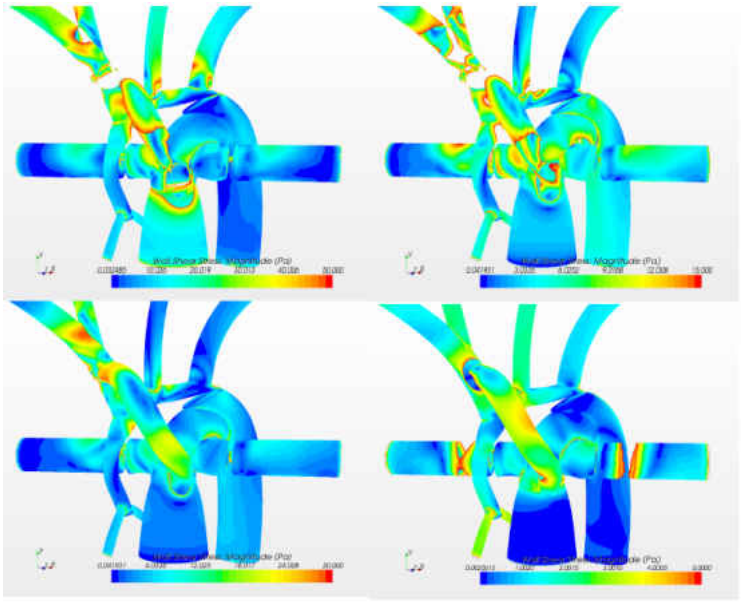

Figure 5.32: Wall Shear Stress Contour Plot of Severe Stenosis with RBTS Configuration

It can be seen in the pressure contour plots that the pressure in the pulmonary root is significantly higher in the severely stenosed case as compared to all cases. This is an area of concern to surgeons since some patients have exhibited hyperplasia in this region due to higher pressure throughout the cardiac cycle. Maintaining higher ventricular pressures also increases strain, fatigue and workload to the heart muscle. In the severely stenosed case with the RBTS in place pressure is similar in magnitude to that of the nominal cases. The velocity vector and streamline plots reveal several areas of flow recirculation and low velocity which are associated with regions of platelet activation and thrombogenesis. The most prominent regions include the root of the innominate and left subclavian artery and also the regions after the pulmonary bandings. In the severe case this effect is exacerbated due to the significant reduction in flow to all arteries, especially those along the ascending and mid aortic arch. Figures 5.25 and 5.29 show flow through the shunt adequately delivers flow to

the innominate artery and ascending aorta. In the severely stenosed case, the shunt delivers about 21% of the cardiac output to the ascending aorta. Of particular interest to surgeons are the areas of flow stagnation, impingement and high/low shear stress. Studies [19] have shown a strong correlation in the magnitude of shear stress, endothelial cell function, and vessel wall remodeling. Low levels of shear stress promote platelet activation and plaque buildup and coincide with areas of low flow velocity, typically the outer walls of bifurcations and recirculation zones. Varying levels of shear stress through the ductus arteriosus, where a metallic stent is placed to prevent it from receding, affect the formation of neointimal hyperplasia and stenosis formation. Flow characteristics surrounding the RBTS anastomosis are also of great interest since there has been early evidence of pulmonary root hyperplasia and studies have suggested there is an optimal shunt diameter as a function of shear stress that achieves greater shunt patency and reduction in graft thrombosis [20]. Figure 5.32 reveals several areas of high shear stress around the the RBTS anostomosis, pulmonary bandings, and ductus arteriosus. Such contour plots can provide guidance to surgeons as they search for more viable ways of implanting the RBTS and pulmonary bandings in order to increase the patient's chances of making a successful recovery[21][22].

CHAPTER 6
CONCLUSIONS AND FUTURE WORK

The multiscale model developed in this study shows its tremendous potential as a predictive tool for surgeons. Detailed local hemodynamics derived from the model provide an insight of the effects of severe stenosis and RBTS implantation. Guidance as to the effects of anatomical changes and shunt placement on local and global hemodynamics can be evaluated using this model. Though the present study mainly concerned changes in the local anatomy, the model can also be used to assess changes in controllable physiological responses affecting peripheral vascular beds, such as cerebral vascular resistance. Patient specific anatomy can also be used instead of the synthetic models to provide analysis on an individual basis. Figure 6.1 shows a 3D reconstruction from CT-Scans performed by this research team of the anatomy of an infant after the Hybrid Norwood procedure. The evolution of the current model is to implement patient specific anatomy with Fluid Structure Interaction algorithms that enable compliance of the walls to be taken into account. A strongly coupled algorithm can thus be implemented and the iterative process developed in this study can be used to provide the initial parameters for various anatomical configurations.

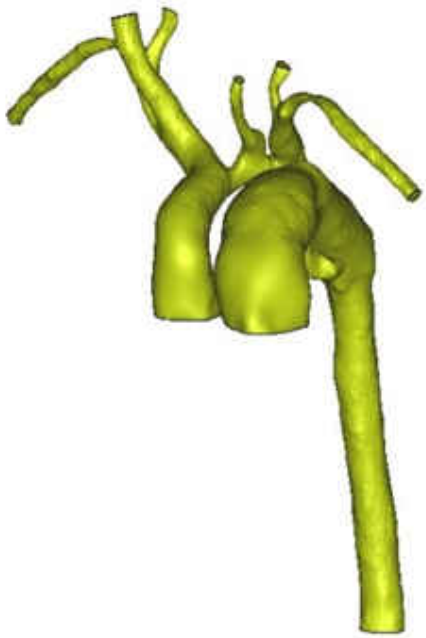

Figure 6.1: 3D Anatomical Reconstruction of Patient After the Hybrid Norwood Procedure

LIST OF REFERENCES

[1] "Hypoplastic Left Heart Syndrome", Digital image. Hypoplastic Left Heart Syndrome. Mayo Foundation for Medical Education and Research. Web. <http://www.mayoclinic.com/health/medical/IM00119>.

[2] "Norwood Procedure for HLHS", Digital image. Treatment for Your Child's Hypoplastic Ventricle: Stage I. Mount Nittany Medical Center. Web. <http://www.mountnittany.org/wellness-library/healthsheets/documents?ID=6702>.

[3] "Hybrid Norwood Anatomy", Digital image. Hybrid Procedures in the Treatment of Congenital Heart Disease. Mayo Foundation for Medical Education and Research. Web. <http://www.mayoclinic.org/images/hybrid-procedures-congenital-heart-1-2col.jpg>.

[4] "Circulatory System", (2009), from National Cancer Institute.

[5] Cohen, B., Taylor, J. and Memmler, R., *Memmler's the structure and function of the human body*, Lippincott Williams & Wilkins (2005).

[6] Levy, M., Pappano, A. and Berne, R., *Cardiovascular physiology*, Mosby physiology monograph series, Mosby Elsevier (2007).

[7] Lloyd-Jones, D., Adams, R., Carnethon, M., De Simone, G., Ferguson, T., Flegal, K., Ford, E., Furie, K., Go, A., Greenlund, K. *et al.*, "Heart disease and stroke statistics–2009 update: a report from the American Heart Association Statistics Committee and Stroke Statistics Subcommittee", *Circulation*, **119**(3), e21 (2009).

[8] Galantowicz, M., Cheatham, J., Phillips, A., Cua, C., Hoffman, T., Hill, S. and Rodeman, R., "Hybrid approach for hypoplastic left heart syndrome: intermediate results after the learning curve", *The Annals of thoracic surgery*, **85**(6), 2063–2071 (2008).

[9] Bacha, E., Daves, S., Hardin, J., Abdulla, R., Anderson, J., Kahana, M., Koenig, P., Mora, B., Gulecyuz, M., Starr, J. *et al.*, "Single-ventricle palliation for high-risk neonates: the emergence of an alternative hybrid stage I strategy", *The Journal of Thoracic and Cardiovascular Surgery*, **131**(1), 163 (2006).

[10] Lagana, K., Balossino, R., Migliavacca, F., Pennati, G., Bove, E., de Leval, M. and Dubini, G., "Multiscale modeling of the cardiovascular system: application to the study

of pulmonary and coronary perfusions in the univentricular circulation", *Journal of biomechanics*, **38**(5), 1129–1141 (2005).

[11] Bacha, E.A. and Hijazi, Z.M., "Hybrid procedures in pediatric cardiac surgery", *Seminars in Thoracic and Cardiovascular Surgery: Pediatric Cardiac Surgery Annual*, **8**(1), 78 – 85 (2005).

[12] Migliavacca, F., Pennati, G., Dubini, G., Fumero, R., Pietrabissa, R., Urcelay, G., Bove, E., Hsia, T. and de Leval, M., "Modeling of the Norwood circulation: effects of shunt size, vascular resistances, and heart rate", *American Journal of Physiology-Heart and Circulatory Physiology*, **280**(5), H2076 (2001).

[13] Barnea, O., Austin, E.H., Richman, B. and Santamore, W.P., "Balancing the circulation: Theoretic optimization of pulmonary/systemic flow ratio in hypoplastic left heart syndrome", *Journal of the American College of Cardiology*, **24**(5), 1376 – 1381 (1994).

[14] Gewillig, M., Boshoff, D., Dens, J., Mertens, L. and Benson, L., "Stenting the neonatal arterial duct in duct-dependent pulmonary circulation: new techniques, better results", *Journal of the American College of Cardiology*, **43**(1), 107–112 (2004).

[15] Suga, H. and Sagawa, K., "Instantaneous pressure-volume relationships and their ratio in the excised, supported canine left ventricle", *Circulation research*, **35**(1), 117 (1974).

[16] Simaan, M., Ferreira, A., Chen, S., Antaki, J. and Galati, D., "A dynamical state space representation and performance analysis of a feedback-controlled rotary left ventricular assist device", *Control Systems Technology, IEEE Transactions on*, **17**(1), 15–28 (2009).

[17] Stergiopulos, N., Meister, J. and Westerhof, N., "Determinants of stroke volume and systolic and diastolic aortic pressure", *American Journal of Physiology-Heart and Circulatory Physiology*, **270**(6), H2050 (1996).

[18] Caldarone, C., Benson, L., Holtby, H. and Van Arsdell, G., "Main pulmonary artery to innominate artery shunt during hybrid palliation of hypoplastic left heart syndrome", *The Journal of Thoracic and Cardiovascular Surgery*, **130**(4), e1 (2005).

[19] Malek, A., Alper, S. and Izumo, S., "Hemodynamic shear stress and its role in atherosclerosis", *JAMA: the journal of the American Medical Association*, **282**(21), 2035 (1999).

[20] Binns, R., Ku, D., Stewart, M., Ansley, J. and Coyle, K., "Optimal graft diameter: effect of wall shear stress on vascular healing.", *Journal of vascular surgery: official publication, the Society for Vascular Surgery [and] International Society for Cardiovascular Surgery, North American Chapter*, **10**(3), 326 (1989).

[21] DeCampli, W., Kassab, A., Argueta, R., Ceballos, A., Divo, E. and Caldarone, C., "Progress Toward Multiscale Modeling of the Hybrid Norwood Circulation", in "Congential Heart Surgeons Society Annual Meeting (2010), Session I: Basic Science & Videos A.", Congential Heart Surgeons Society.

[22] Ceballos, A., Osorio, R., Kassab, A., Divo, E. and DeCampli, W.M.and Argueta, R., "A Multiscale Model of the Neonatal Circulation Following Hybrid Norwood Palliation", in "Proceedings of the Fourth International Conference on Computational Methods for Coupled Problems in Science and Engineering, ECCOMAS, Kos, Greece[CD-Rom]", (2011).